Identification of Common and Separate Mechanisms Governing Circadian Locomotor Activity and Body Temperature

（行動と体温の概日変動を支配する共通および個別メカニズムの同定）

2020

嶋谷　寛之

Contents

Preface

Almost all organisms, including humans, display daily rhythms of behaviour and physiology generated by an endogenous mechanism called circadian clock. In mammals, these rhythms are established by transcription/translation-based autoregulatory feedback loops, in which non-coding *cis*-regulatory elements on the promoter of the clock genes are believed to play a key role in generating circadian transcription. Genetic evidence supporting this model, however, is still exclusively based on the effects of mutations in the protein-coding sequences of the clock genes. Therefore, while non-coding circadian *cis*-elements are assumed to be important for daily maintenance of behaviour and physiology, there is currently no direct evidence to corroborate this notion.

Because locomotor activity rhythms (LAR) and body temperature rhythms (BTR) are both robust and easy to be measured, they have been used to detect circadian rhythms in living animals. Interestingly, BTR is separately regulated from LAR, and BTR has essential roles in maintaining circadian energy homeostasis and entrainment of peripheral tissue clocks. A previous study, in which subsets of neurons in the brain of rats were ablated, suggested that LAR and BTR are controlled by different output pathways that originate from the suprachiasmatic nucleus (SCN). However, molecules involved in regulating BTR have not been identified so far.

Methodologically, there are several critical problems in measurements of BTR. In many studies, BTR measurements were usually performed by surgical implantation of a thermal sensor into abdominal cavity of animals. Moreover, a sensor device is often large for small laboratory animals, such as mice, making these experiments highly invasive. In addition, long-term measurement of BTR with high time-resolution over several days is difficult due to limited data storage performance of thermal sensor devices. LAR is usually detected by infrared sensor, but this conventional method also has several limitations. Firstly, it is difficult to accurately quantify locomotor activities because the sensitivity differs between infrared sensor devices, and the sensitivity changes gradually over time due to mechanical degradation. Secondly, mice often show non-locomotor activities, such as feeding, grooming, and postural adjustments, but these subtle changes in activity cannot be distinguished via a conventional infrared sensor. These limitations have hampered elucidation of whether and how BTR and LAR are temporally related to each other.

In Chapter 1, using mice with a point mutation in the *cis*-regulatory element E′-box in the promotor region of *Period2* (*Per2*), I showed that circadian transcription of *Per2* and other clock genes was drastically attenuated in cells derived from the mutant mice, indicating that circadian core clock cycling is achieved through the *Per2* E′-box. Furthermore, these mutant mice cannot maintain proper LAR and BTR. **In Chapter 2**, I showed that the calcitonin receptor, a G-protein coupled receptor (GPCR) that is abundantly expressed in the SCN, is involved in BTR control without affecting LAR. **In Chapter 3**, I established a new method for simultaneous measurement of body movements and body surface temperature (BST) using an infrared camera to elucidate their detailed temporal relationship.

Chapter 1: Non-coding *cis*-element of *Period2* is essential for maintaining organismal circadian behaviour and body temperature rhythmicity

To determine whether *cis*-element-mediated transcription/translation-based feedback loops is required for the formation of the circadian clock, I focused on the E'-box located near the transcriptional start site of *Per2*. I found that the mutation of the *Per2* E'-box attenuated the circadian rhythms of cultured cells and tissues, and prevented mice from maintaining proper circadian rhythms in locomotor activity and body temperature. These results provide the first genetic evidence that non-coding element-based *Per2* transcription is essential for generating cell-autonomous clock and for maintaining organismal circadian behaviour and body temperature rhythmicity.

Chapter 2: Calcitonin receptor modulates body temperature rhythms in mammals

The neurons in the hypothalamic SCN, the center of the body circadian clock, are known to project to various brain regions and involved in shaping circadian rhythms of many behavioural and physiological states. However, their molecular mechanisms are largely unknown. The calcitonin receptor (*Calcr*) is a GPCR that is abundantly expressed in the SCN, but its contribution to BTR has been completely unknown. To elucidate the role of *Calcr*, I simultaneously measured BTR and LAR of *Calcr*-deficient mice. LAR of *Calcr*-deficient mice were comparable to that of wild-type mice. However, BTR of *Calcr*-deficient mice are significantly different from that of wild-type mice. BTR of wild-type animal normally displays bimodal two peaks, one in the early night and at dawn, with a deep trough at midnight. By contrast, BTR of *Calcr*-deficient mice lacked this characteristic dip at midnight and remained relatively unchanged throughout the night. Thus, I have identified for the first time a molecule involved in mid-night BTR control without affecting LAR.

Chapter 3: Temporal relationships between body temperature and behaviour revealed by thermographic imaging

To elucidate the temporal relationship between behaviour and body temperature in mice, I developed a method that enables simultaneous tracing of body movements and body surface temperature (BST). To this end, I used infrared video camera. It is known that locomotor activity and body temperature are highly correlated; basically, body temperature is high when animals are locomotorily active. As a result, locomotion is considered to elevate body temperature. However, I found that changes in BST are not always associated with changes in locomotor activity. Interestingly, video analysis revealed that mice exhibit non-locomotor activities just before start of locomotion and that BST is increased in association with these non-locomotor activities. I also found that significant BST variations occur even when animals are at rest. Thus, my thermographic video imaging identified thermoregulation which is independent of locomotor activities.

Chapter 1

Non-coding *cis*-element of *Period2* is essential for maintaining organismal circadian behaviour and body temperature rhythmicity

Introduction

Evidence shows that non-coding *cis*-regulatory elements are as important as protein-coding sequences for determining cell identity and morphological development[1-3]. The degree of the effects of non-coding *cis*-regulatory elements on animal behaviour and physiology after development, however, remains elusive. Circadian clocks generate ~24 h rhythms in behaviour and physiology, which allow organisms to anticipate and adjust to daily environmental changes. The rhythm generating mechanism of the circadian clock involves clock genes, which regulate their own transcription in a negative transcription-translation feedback loop[4-6]. In this canonical feedback model, non-coding *cis*-elements are fundamental to both initiating and closing the loop[7-9]. Genetic evidence supporting this model, however, is still exclusively based on the effects of mutations in the protein-coding sequences of the clock genes. Therefore, while it is tempting to speculate that the circadian clock-related non-coding *cis*-elements are operational for daily dynamic regulation of behaviour and physiology, there is currently no direct evidence to corroborate this notion.

Notwithstanding the recent intriguing discoveries of circadian oscillations in peroxiredoxin superoxidation in transcriptionally incompetent anucleate erythrocytes[10] and the expression of such cycles in the neurons in the suprachiasmatic nucleus (SCN)[11], the consensus conjecture regarding the mammalian clockwork supports the transcriptional feedback model. However, the literature addressing mutations or deletions in the protein-

coding sequences of the clock genes cannot negate the possible contribution of post-translational (or non-genomic) clock mechanisms. Moreover, the extent of the impact of the *cis*-regulated transcriptional feedback cycle on establishing circadian rhythmicity in vivo remains the subject of considerable debate[4,12], due in large part to the lack of genetic research on non-coding *cis*-element mutations. In a recent study, our laboratory developed mutant mice carrying a mutation in a circadian *cis*-acting element of the core clock gene *Per2*[13]. Although *Per2* was cloned as a secondary period gene in mammals, gene knockout studies revealed that *Per2* mutant mice displayed a loss of circadian rhythmicity, revealing its prominent role in the mammalian molecular clockwork[14-16]. Moreover, familial advanced sleep phase syndrome in humans is attributed to a missense mutation in the *Per2* gene[16].

The *Per2* E′-box sequence (5′–CACGTT–3′) located near the putative transcription initiation site[18] (–20 to –15) has been demonstrated to be the principal circadian *cis*-element that is sufficient to induce oscillating levels of reporter transcription via the mouse *Per2* minimal promoter[18,19]. The importance of this particular *cis*-element is further implied by the high degree of DNA sequence conservation in its flanking region between humans and mice[18] and by extremely enriched clock protein binding to this element. Publicly[20] available genome-wide ChIP-seq data highlight the predominant peak of clock protein binding activity around this E′-box.

The present study was designed to investigate the role of this unique E′-

box sequence of the *Per2* promoter (hereafter, *Per2* E′-box) as a potential nodal *cis*-element in the mammalian clockwork. By using mice which are introduced a site-specific mutation at this element, I provide empirical evidence to show that the *Per2* E′-box is essential for maintaining cell-autonomous circadian oscillations. The cells without the *Per2* E′-box cannot maintain circadian molecular oscillations under culture conditions. At the organismal level, mice lacking the *Per2* promoter E′-box show destabilized LAR and BTR under altered light conditions, including constant light (LL) and experimental jet-lag conditions. Due to compensatory mechanisms in vivo, the mutant mice kept under constant dark (DD) conditions remain rhythmic but exhibit considerably shorter circadian periods than WT mice. My data therefore define the degree of the impact of the deletion of the *Per2* E′-box on the organismal clock: The *Per2* E′-box is essential for the period determination of behavioural rhythms in DD conditions and for sustaining stable rhythms under LL and jet-lag conditions. These data underscore the roles of the non-coding *cis*-element in the regulation of daily behaviour and physiology in adulthood.

Methods

Mouse strain

*Per2*E′$^{m/m}$ mice were as described before[13]. Where specified, *Per2*E′$^{m/m}$ mice were intercrossed with mice carrying a *Bmal1-Eluc* reporter[21-23] and/or *Per1*-

deficient mice[15] of C57BL/6J background (The Jackson Laboratory, 10491). All animal experiments were conducted in compliance with ethical regulations in Kyoto University and performed under protocols approved by the Animal Care and Experimentation Committee of Kyoto University.

Cell culture and immunoblotting

WT and *Per2*E′$^{m/m}$ primary fibroblasts were isolated from the lung tissue of adult male mice according to a protocol established by Seluanov et al[24]. Cells used for time course assay were between passages 4 and 6. Dispersed cells were uniformly plated in 24-well plates at a density of 1 × 105 cells per well and cultured for 2 days prior to synchronization, for which cells were treated with dexamethasone (DEX, final concentration, 200 nM) for 3 h, followed by medium refreshment at Time0. Cells were harvested every 4 h in either TRIzol reagent (Invitrogen) for RNA analysis or 2 × Laemmli buffer for Western blot analysis. Immunoblotting was performed using an affinity-purified anti-mPER2 rabbit polyclonal antibody[25] (final concentration, 2 μg ml−1) and β-Actin antibody (A5441, Sigma, 1:1000).

RNA extraction and RT-qPCR

Total RNA was extracted with RNeasy kit (Qiagen) and converted to cDNA with SuperScript VILO cDNA Synthesis kit (Invitrogen). qPCR was run on a BioMark HD System (Fluidigm) with a 48.48 Fluidigm BioMark Dynamic Array chip (Fluidigm)[26]. TaqMan probe and primer sets were as follows; for

Per2, probe, FAM-AGG CAC CTC CAA CAT GCA ACG AGC C-TAMRA, forward primer (fw): 5′-GCA CAT CTG GCA CAT CTC GG-3′, reverse primer (rv): 5′-TGG CAT CAC TGT TCT GAG TGT C-3′; for *Per2* intron, probe, FAM-TGG AGC CCA CCG CAG ACA GCC C-TAMRA, fw: 5′-CCT CTC ACC TCA TGC CCT TTT AG-3′, rv: 5′-CTG CTC AGA CCA ACA GAT TTA TCA-3′; for *Per1*, probe, FAM-AGC CCC TGG CTG CCA TGG-TAMRA, fw: 5′-CAG GCT TCG TGG ACT TGA GC-3′, rv: 5′-AGT GGT GTC GGC GAC CAG-3′; for *Per3*, probe, FAM-TTC TGC TCA TCA CCA CCC TGC GGT TCC-TAMRA, fw: 5′-ACA GCT CTA CAT CGA GTC CAT G-3′, rv: 5′-CAG TGT CTG AGA GGA AGA AAA GTC-3′; for *Cry1*, probe, FAM-TGA TCC ACA GGT CAC CAC GAG TCA GGA A-TAMRA, fw: 5′-TAG CCA GAC ACG CGG TTG-3′, rv: 5′-AGC AGT AAC TCT TCA AAG ACC TTC A-3′; for *Cry2*, probe, FAM-AGG TCT CTC ATA GTT GGC AAC CCA GGC-TAMRA, fw: 5′-TGG ACA AGC ACT TGG AAC GG-3′, rv: 5′-GGC CAG TAA GGA ATT GGC ATT C-3′; for *Clock*, probe, FAM-ACC CAG AAT CTT GGC TTT TGT CAG CAG C-TAMRA, fw: 5′- TGG CAT TGA AGA GTC TCT TCC TG-3′, rv: 5′-GAG ACT CAC TGT GTT GAT ACG ATT G-3′; for *Bmal1*, probe, FAM-CGC CAA AAT AGC TGT CGC CCT CTG ATC T-TAMRA, fw: 5′-GTA CGT TTC TCG ACA CGC AAT AG-3′, rv: 5′-GTA CCT AGA AGT TCC TGT GGT AGA-3′; for *Nr1d1*, probe, FAM-CCC TGG ACT CCA ATA ACA ACA CAG GTG G-TAMRA, fw: 5′-TCA GCT GGT GAA GAC ATG ACG-3′, rv: 5′-GAG GAG CCA CTA GAG CCA ATG-3′; for *Dbp*, probe, FAM-CGG CTC CCA GAG TGG

CCC GC-TAMRA, fw: 5′-CGG CTC TTG CAG CTC CTC-3′, rv: 5′-GTG TCC CTA GAT GTC AAG CCT G-3′; for *E4bp4*, probe, FAM-CAG GGA GCA GAA CCA CGA TAA CCC ATG A-TAMRA, fw: 5′-CGC CAG CCC GGT TAC AG-3′, rv: 5′-CAT CCA TCA ATG GGT CCT TCT G-3′; for *Rplp0*, probe, FAM-TGG CAA TCC CTG ACG CAC C GC C-TAMRA, fw: 5′-GCG TCC TCG TTG GAG TGA C-3′, rv: 5′-AAG TAG TTG GAC TTC CAG GTC G-3′. for *Gapdh*, probe, FAM-CGG CCA AAT CCG TTC ACA CCG ACC-TAMRA, fw: 5′-GAG ACG GCC GCA TCT TCT T-3′, rv: 5′-TCT CCA CTT TGC CAC TGC A-3′. Values were normalized to average expression of *Rplp0* and *Gapdh*.

Real-time bioluminescence recording and data analysis

Tissues from mice carrying a *Bmal1* promoter-driven luciferase reporter (*Bmal1-ELuc*)[21] were harvested from adult (2–3 months-old) male mice between ZT10–12 and cultured according to a published method[27]. In brief, brains were sliced coronally into 400-μm sections, and the paired SCN, which contains minimal volumes of the non-SCN, were cultured[28]. The lungs were cut into a small piece (~2 × 2 × 0.3 mm^3)[28]. The adrenal glands were sliced into a section of 0.3 mm thickness. All tissues were cultured separately on a Millicell membrane (PICMORG50, Millipore) with DMEM medium containing10 mM HEPES (pH 7.2), 2% B27 (Invitrogen) and 1 mM luciferin, in 35-mm dish, and air sealed. Bioluminescence recording was started immediately upon placement in culture with a dish-type luminometer

(Kronos Dio, ATTO) maintained at 37 °C. Luminescence was measured for 3 min for each dish at 30-min intervals. The data were smoothed using a 2 h moving average and further detrended by subtracting a 24 h running average for FFT analysis. A fourth-order Blackman–Harris window was applied before the power spectrum calculation. The spectrum was normalized to an integral of one by dividing each of its elements by the sum of all elements. Circadian rhythmicity was defined as relative spectral power density at the peak in the circadian range (20–30 h). The peak values represent the power within a frequency band of 0.009.

Locomotor activity recording and data analysis

C57BL/6J-backcrossed *Per2*E′$^{m/+}$ mice were intercrossed to produce homozygous mutant (*Per2*E′$^{m/m}$) and WT (*Per2*E′$^{+/+}$) progenies using in vitro fertilization. We used adult male mice (8- to 10-week old). The animals were housed individually in light-tight, ventilated closets under indicated lighting conditions with ad libitum access to food and water. Locomotor activity was recorded via passive infrared sensors (PIRs, FA-05F5B; Omron) with 1-min resolution and analyzed with CLOCKLAB software (Actimetrics)[29]. Free-running period in DD was determined with $\chi 2$ periodogram, based on animal behaviours in a 40-day interval taken 3 days after the start of DD condition. Rhythmicity in LL was evaluated using FFT-Relative Power (CLOCKLAB, Actimetrics). A fourth-order Blackman–Harris window was applied before the power spectrum calculation. The spectrum was normalized to an integral

of one by dividing each of its elements by the sum of all elements. Circadian rhythmicity was defined as relative spectral power density at the peak in the circadian range (20–36 h). The peak values represent the power within a frequency band of 0.006. Speed of behavioural re-entrainment was evaluated using 50% phase-shift value (PS_{50})[31,32]. To determine PS50, sigmoidal dose-response curve with variable slope, $Y = Bottom + (Top – Bottom)/(1 + 10^{(\log PS50 – X) HillSlope})$, was fitted to the onset time points using GraphPad Prism software. Body temperature recording and data analysis. Precalibrated temperature data loggers (Thermochron iButtons, DS1921H, Maxim) were surgically implanted to the peritoneal cavity of mice under general anaesthesia. After a week of recovery in LD, mice were transferred into LL. The iButtons were programmed for collecting temperature data every 20 min. For data analysis, the mean temperature of the entire data series during days 7 to 21 in LL was calculated, and the data points above the mean were displayed in double-plotted format using CLOCKLAB. For circular plot, data were detrended by subtracting a 24 h running average, and periods of top 20% temperature were deployed in Rayleigh format using Oriana 4 software (Kovacs Computer Services, UK). CT12 was extrapolated from the onsets of locomotor activity during days 3–6. Phase distribution was assessed by mean vector length (Oriana 4).

Results

Per2 E′-box is essential to maintain cellular circadian oscillations

To investigate the role of the *Per2* E′-box in maintaining cellular oscillation, I generated primary fibroblast cultures from lung tissues of WT (*Per2*E′$^{+/+}$) and *Per2* E′-box mutant (*Per2*E′$^{m/m}$) mice[13], and monitored circadian fluctuations in the PER2 protein levels over 80 h (Fig. 2a). As expected, the endogenous PER2 protein in synchronized WT cells displayed characteristic circadian oscillations in both abundance and electrophoretic mobility, which continued over multiple cycles under constant culture conditions[25] (Fig. 1a). In contrast, *Per2*E′$^{m/m}$ cells failed to maintain normal PER2 protein oscillations (Fig. 1a). It is important to note that the mutant cells could competently form the first surge of PER2 expression after synchronization (4–12 h). However, following a subsequent increase (28 h), PER2 expression in the mutant cells remained at mid-to-high levels and eventually lost apparent circadian variation after 60 h. Electrophoretic migration rhythms also disappeared from the mutant cells (Fig. 1a). The relative intensities of the three major bands of the PER2 protein remained unchanged in the *Per2*E′$^{m/m}$ cells. The post-translational rhythms were thus affected either directly or indirectly by the mutation of the E′-box. I experimentally confirmed that the protein-coding sequences of PER2 and known clock protein kinases and phosphatases were unaffected in the mutant mice. These results indicate that the E′-box is indispensable for maintaining normal PER2 protein oscillations.

In the *Per2*E′$^{m/m}$ cells, I observed that both *Per2* mRNA and pre-mRNA (intronic RNA) levels remained constitutively high, with values exceeding those of the circadian peak in the WT cells at 72 h (Fig. 1b). Thus, *Per2* transcription remains active even without this particular E′-box sequence in the promoter. Moreover, extensive mRNA profiling revealed that the effects of the mutation of the *Per2* E′-box were not limited to *Per2* transcription. The dysfunctional *Per2* E′-box also abolished the circadian expression of other clock genes and output genes, including *Per1*, *Per3*, *Cry1*, *Cry2*, *Bmal1*, *Nr1d1*, *Dbp*, and *E4bp4* (Fig. 1b). These pervasive effects of the mutation provide evidence that the *Per2* E′-box is a fundamental *cis*-element that maintains normal molecular clock oscillations.

Per2 E′-box is essential to maintain molecular oscillations in the SCN

The SCN in the hypothalamus is the primary regulator of daily rhythms of behaviour and physiology in mammals[32,33]. I next examined the effect of the *Per2* E′-box mutation on the SCN clock. To study the molecular rhythms in the SCN, I used a *Bmal1* promoter-driven luciferase reporter (*Bmal1-Eluc*)[21], as it allowed the assessment of molecular rhythms that are not a simple reflection of the *Per2* loop. In agreement with previous reports[22], organotypic SCN slices prepared from control mice (*Per2*E′$^{+/+}$; *Bmal1-Eluc*) displayed persistent circadian rhythms of luminescence, which continued for over a week in culture (Fig. 2a). In contrast, all tested SCN slices from the *Per2* E′-box mutant mice (*Per2*E′$^{m/m}$;*Bmal1-Eluc*) displayed attenuated

rhythms of luminescence, which were damped within 2–3 cycles (Fig. 2a). Fast Fourier transform (FFT) analysis of the de-trended waveforms of days 1.5−7.5 (Fig. 2b) confirmed the reduced rhythmicity in the *Per2*E′$^{m/m}$ SCN. This finding indicated the relevance of the *Per2* E′-box in maintaining normal molecular circadian oscillations in the SCN. Nevertheless, detectable rhythms were noted in the attenuated *Per2*E′$^{m/m}$ SCN slices over the initial 2–3 cycles (Fig. 2a). These remaining rhythms were likely dependent on *Per1*, because SCN explants from *Per2*E′$^{m/m}$;*Per1* heterozygous null mice (*Per2*E′$^{m/m}$; *Per1*$^{+/-}$;*Bmal1-Eluc*) exhibited even fewer persistent rhythms, which were damped within 2 cycles (Fig. 2a–c). Importantly, similar attenuation of *Bmal1-Eluc* rhythmicity by *Per2*E′$^{m/m}$ and further by *Per1*$^{+/-}$ could be reproduced in cultures of lung (Fig. 2d–f), confirming the importance of the *Per2* E′-box in keeping sustained molecular circadian oscillations not only for the SCN but also for the peripheral tissues.

Destabilized organismal rhythms of animal lacking *Per2* E′-box

Finally, to assess the effects of the mutation at the behavioural level, C57BL/6J-backcrossed WT and *Per2*E′ m/m mice were housed in a 12-h light:12-h dark (LD) cycle and then subjected to DD, LL, or experimental jet-lag conditions. Actograms of the animals in the respective conditions were acquired. Interestingly, mutant mice kept in DD showed overt circadian LAR, although with a significantly shortened free-running circadian period relative to WT mice (WT vs. Per2E′$^{m/m}$: 23.71 ± 0.02 h vs. 23.50 ± 0.02 h;

see Supplementary Fig. 1). This contrast with the in vitro data suggests that a compensatory mechanism functions in vivo. I thus examined the circadian behaviour of *Per1*$^{-/-}$;*Per2*E′$^{m/m}$ double-deficient mice (see Supplementary Fig. 2). Although their period length was unstable and changed gradually over extended exposure to constant darkness, *Per1*$^{-/-}$;*Per2*E′$^{m/m}$ mice displayed behavioural rhythms over 40 days. With analogy, *Drosophila* strains expressing *period* or *timeless* under a constitutive promoter were reported to show behavioural rhythms with an altered period length[12,34]. These data suggest that organisms might have a compensatory mechanism to mitigate defective transcriptional feedback regulation[4,32,35].

Compared to the modest phenotype in DD, I observed unstable rhythmicity of the mutant mice in LL (Fig. 3a). When placed in LL for 3 weeks, WT subjects (n = 7) stayed rhythmic with a period longer than 24 h, which is consistent with data from previous reports[36,37]. However, none of the *Per2*E′$^{m/m}$ mice (n = 9) remained rhythmic (Fig. 3a); all tested mutant mice displayed behaviours characterized by a gradual decrease in the power of rhythmicity (FFT spectrogram, Fig. 3a). Since light has a negative masking effect on locomotor activity, I measured core body temperature fluctuations and confirmed that the body temperature recapitulated the reduced rhythmicity of the mutant mice in LL conditions (Fig. 3b, Rayleigh vector length of WT vs. *Per2*E′$^{m/m}$: 0.64 ± 0.06 vs. 0.42 ± 0.02).

The *Per2* E′-box mutant mice were also distinct under experimental jet-lag conditions (Fig. 3c). When the ambient LD cycle was advanced by 8 h,

WT mice re-entrained progressively over 8 to 9 days[30]. In contrast, the *Per2*E′$^{m/m}$ mice adapted to the new cycle within 2–3 days. The 50% phase-shift value (PS50)[30], measured from activity onset, indicated a rapidity of 5.33 ± 0.28 days for WT mice and 1.26 ± 0.17 days for *Per2*E′$^{m/m}$ mice (Fig. 3c). Notably, the difference between the two genotypes was even pronounced when the animals were exposed to a single 8-h light advance, followed by DD conditions (Fig. 3d). Under this light regime, all tested mutant mice shifted forward by approximately 12 h, which is nearly 180° out of phase in a 24-h cycle, relative to WT mice (Fig. 3d). The underlying mechanism of this extremely large shift is unknown. While this could be due to an indirect effect of the weak clock, a limit cycle oscillator model[38] predicts that a reduced-amplitude pacemaker in the mutant mice (reduced radius of the limit cycle) could have this effect[39]. I also noticed that after a light pulse exposure, the mutant mice show a slightly enhanced *Per2* mRNA induction in the SCN (see Supplementary Fig. 3). This perhaps also partly contributes to the enhanced resetting of the mutant mice.

Discussion

Non-coding *cis*-regulatory elements are known to play a critical role in development, but their precise effects on daily behaviour and physiology in adulthood remain elusive. The present study was designed to provide genetic evidence for the roles of the circadian *cis*-element in vivo. Despite the

presence of compensatory mechanisms in vivo, my work shows that the *Per2* E′-box is essential for maintaining optimal LAR under LL conditions and enabling the phase of the clock to resist abrupt shifts in LD cycling. In general, adapting to new LD cycles is rarely instantaneous and requires repeated 24 h cycles. However, the *Per2* E′-box mutant mice adapted to a new phase immediately. These data elucidate the impact of the deletion of the non-coding *cis*-element in daily maintenance of behavioural activity in adulthood.

In addition, the cell culture data presented here reinforce the concept that circadian clock phenotypes are more drastic at the cellular level than the organismic level[4,32]. The *Per2* E′-box mutation leads to unsustainable gene expression rhythms in organotypic SCN slices and cultured peripheral tissues and fibroblasts. These observations substantiate the general conjecture that *cis*-regulatory element-based gene transcription is essential for sustaining cellular clock oscillations.

Not surprisingly, the overall behavioural phenotypes of the *Per2* E′-box mutant mice reveal that the *Per2* E′-box is not an absolute requirement for behavioural rhythm generation. Under DD conditions, its deletion affects only the circadian period, a phenotype analogous to that observed in transgenic *Drosophila* strains expressing *period* or *timeless* via a constitutive promoter[12,34]. At the gene expression level, *Per2* expression in the liver and SCN in the DD-kept mutant mice in vivo was still rhythmic, albeit with an increased baseline[13]. These observations suggest that organisms have a

compensatory mechanism to mitigate defective transcriptional feedback regulation. Correspondingly, previous studies demonstrate that behavioural rhythms do not necessarily reflect cellular clock phenotypes[35,40-42]; superior circadian performance of behavioural rhythmicity has been observed in several clock gene mutant mice, compared to tissue cultures obtained from the same animal strains[35]. In vivo multicellular and/or inter-organ systemic circuitry might compensate for poor core clock function within individual cells[4]. In this regard, it is worth noting that systemic extracellular signals are known to affect the *Per2* promoter via non-E′-box *cis*-regulatory elements, such as cAMP response element (CRE)[43] and glucocorticoid response element (GRE)[44]. Extracellular circadian feedback pathways through these non-E′-box elements might contribute to the compensatory mechanisms in vivo[45,46].

This study differs from transgenic studies, in which non-native promoters are used[12,18]. Transgenic studies and rescue experiments can be affected by shorter promoter regulatory sequences and position effects. In comparison, native promoters are characterized by endogenous enhancer elements and normal chromatin structure, allowing for the preservation of regulation by epigenetic factors, which are known to be crucial for controlling transcription. Under these near-native conditions, I noticed that the deletion of the *Per2* E′-box leads to accumulation of *Per2* mRNA and protein in cultured fibroblasts. Constitutively un-suppressed transcription of *Per2* likely underlies the constant accumulation of the PER2 protein and

resultant compromised gene expression rhythms in the mutant cells.

Cis-element provides a place where both active and repressive transcription complexes are recruited. The net effect of its absence thus seems context-dependent. The question of this context specificity is still unresolved in the field of transcription and chromatin remodeling. Particularly, in the case of this study, the mechanism(s) that allows the continued transcription of *Per2*[9,19,47] without relying on the E′-box is still unknown. It is possible that native chromatin structure of the *Per2* might permit its transcription. It is also conceivable that other circadian *cis*-elements on the *Per2* promoter, such as D-box and CRE, might contribute to the basal transcription of *Per2*. In this regard, the continued expression of *Per2* might reflect a confounding effect of being chronically deficient in the functional E′-box. Given that *Per2* is under regulation of interlocked feedback cycles[6,9], remaining *Per2* transcription might be a homeostatic consequence of a nonfunctional clock in the mutant cells. A complete understanding of circadian regulation of *Per2* in vivo under native conditions remains a challenge for future study.

Genome-wide association studies recently identified many non-coding variants that account for human chronotypes[48-50]. Given the physiologic relevance of the *Per2 cis*-element, a targeted point mutation strategy would facilitate hypothesis-driven approaches to understand the extent of the impact of the non-coding elements on the daily physiology and pathophysiology of the organism.

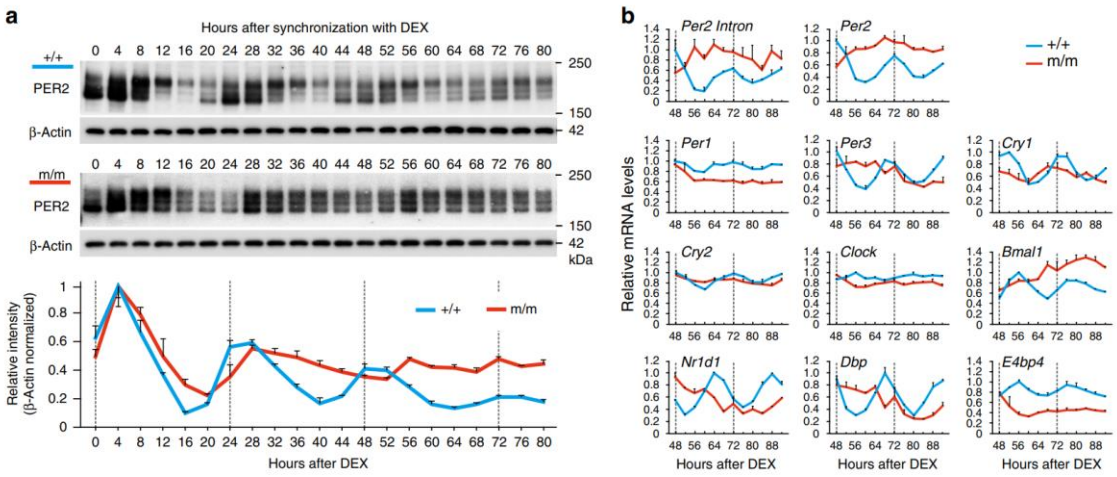

Fig. 1 *Per2* E′-box is essential for maintaining cell-autonomous circadian oscillations. (**a)** Temporal profiles of PER2 protein expression in *Per2*E′$^{+/+}$ and *Per2*E′$^{m/m}$ fibroblasts. Representative immunoblots and normalized densitometry values (n = 3, mean ± s.e.m.) are shown. (**b)** mRNA profiling of clock genes in *Per2*E′$^{+/+}$ and Per2E′$^{m/m}$ fibroblasts (n = 2, for each data point). For *Per2*, both intron and exon RNA were analyzed. The data are presented as the mean ± variation.

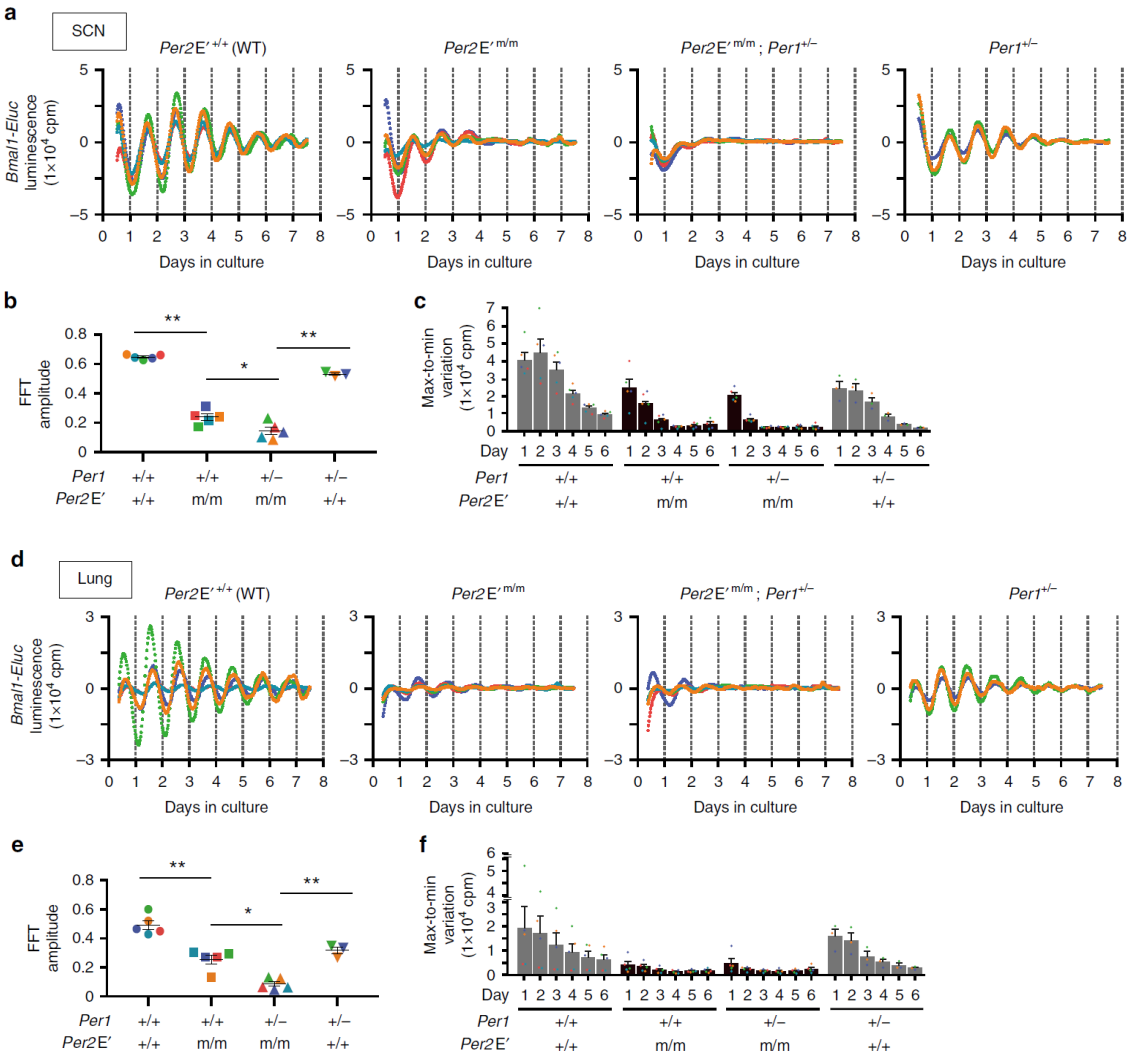

Fig. 2 *Per2* E′-box is essential for sustainable *Bmal1* oscillations in SCN and lung explants. **a** *Bmal1-Eluc* bioluminescence traces of ex vivo SCN cultures from *Per2*E′$^{+/+}$ ($n = 5$), *Per2*E′$^{m/m}$ ($n = 5$), *Per2*E′$^{m/m}$; *Per1*$^{+/-}$ ($n = 5$), and *Per1*$^{+/-}$ ($n = 3$) mice. Averaged de-trended data are shown. **b** FFT amplitude of (**a**). *$P < 0.05$, **$P < 0.001$, one-way ANOVA, Bonferroni post hoc test. **c** Daily max-to-min variations of (**a**). The data are presented as the mean ± s.e.m. **d** *Bmal1-Eluc* bioluminescence traces of lung tissue explant cultures from *Per2*E′$^{+/+}$ ($n = 5$), *Per2*E′$^{m/m}$ ($n = 5$), *Per2*E′$^{m/m}$; *Per1*$^{+/-}$ ($n = 5$), and *Per1*$^{+/-}$ ($n = 3$) mice. Averaged de-trended data are shown. **e** FFT amplitude of (**d**). *$P < 0.05$, **$P < 0.001$, one-way ANOVA, Bonferroni post hoc test. **f** Daily max-to-min variations of (**d**). The data are presented as the mean ± s.e.m.

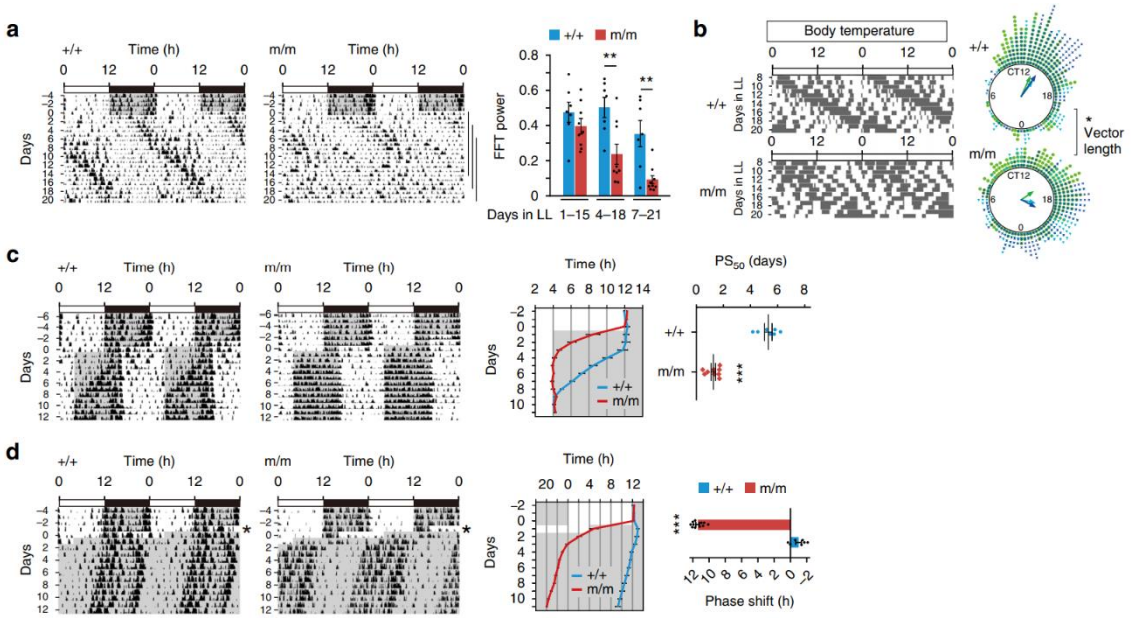

Fig. 3 **a** Destabilized circadian LAR and BTR of *Per2* E′-box mutant mice. Representative locomotor activity records of *Per2*E′$^{+/+}$ and *Per2*E′$^{m/m}$ mice under light/dark (LD) followed by constant light (LL). The graph shows changes in FFT power in LL. $^{**}P < 0.01$, two-way repeated-measures ANOVA, Bonferroni post hoc test (*Per2*E′$^{+/+}$, $n = 7$; *Per2*E′$^{m/m}$, $n = 9$). **b** Representative body temperature records of *Per2*E′$^{+/+}$ and *Per2*E′$^{m/m}$ mice in LL. The mean temperature of the entire data series was calculated, and the data points above the mean are plotted. Rayleigh plots show phase distribution of elevated body temperature on days 7–21 ($n = 3$, each genotype). Data from independent animals are color-coded. Arrow length reflects the *r*-value of each distribution. $^{*}P < 0.05$, two-tailed unpaired *t*-test. **c** Representative records of locomotor activity (left) and plots of activity onset (middle) of *Per2*E′$^{+/+}$ and *Per2*E′$^{m/m}$ mice before and after an 8-h phase advance in LD cycles. The PS_{50} values represent the time required for 50% phase-shift (right). $^{***}P < 0.0001$, two-tailed unpaired t-test (*Per2*E′$^{+/+}$, $n = 7$; *Per2*E′$^{m/m}$, $n = 9$). **d** Representative locomotor activity records (left), activity onset (middle), and magnitude of phase-shift (right) of *Per2*E′$^{+/+}$ and *Per2*E′$^{m/m}$ mice subjected to an 8-h phase advance on day 1 and released to DD. $^{***}P < 0.0001$, two-tailed unpaired *t*-test (*Per2*E′$^{+/+}$, $n = 7$; *Per2*E′$^{m/m}$, $n = 11$).

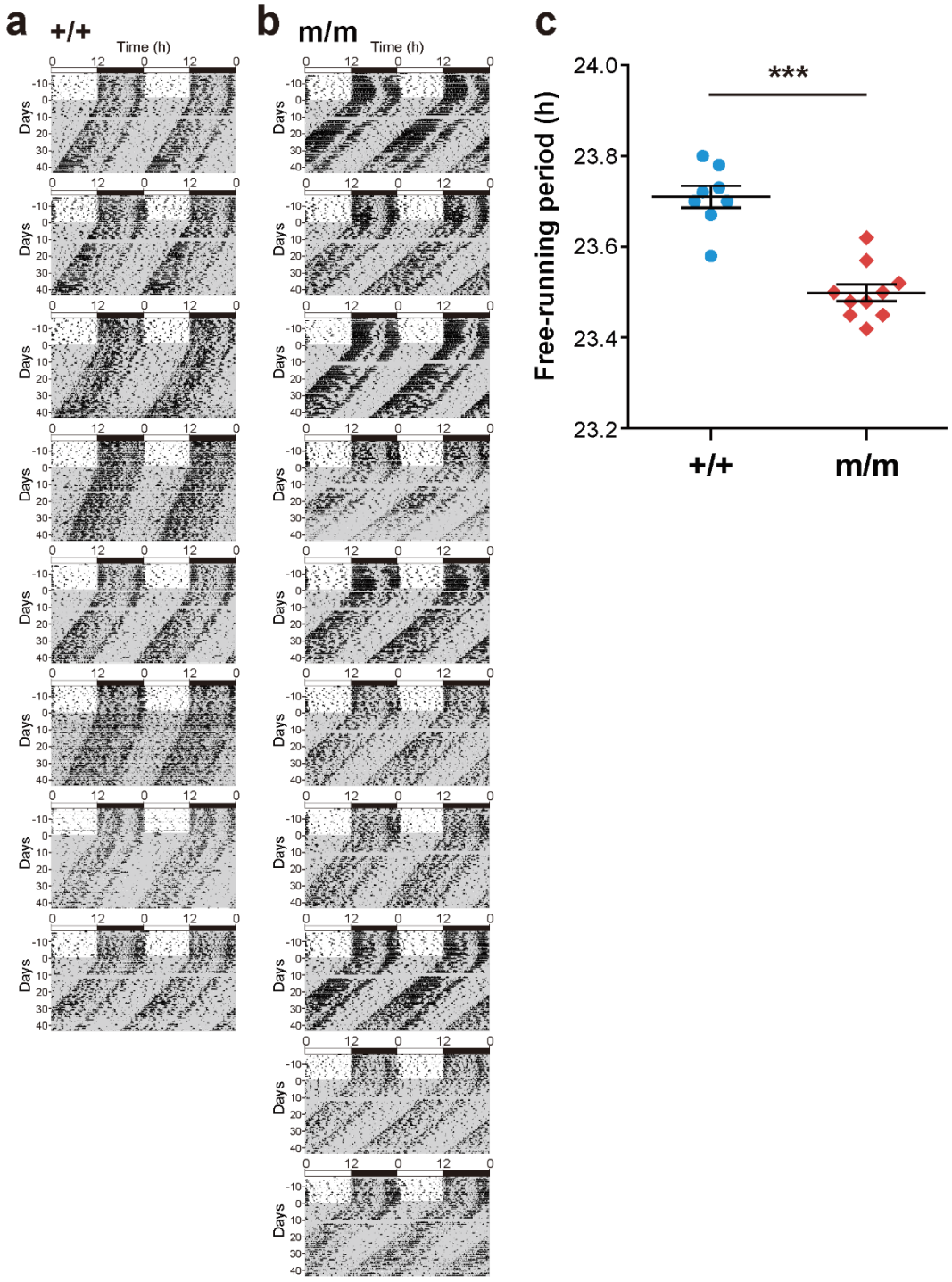

Supplementary Fig. 1 *Per2*E′$^{m/m}$ mice display a short free-running period of locomotor activity rhythms in DD. Double-plotted actograms of WT (**a**) and *Per2*E′$^{m/m}$ (**b**) mice. Animals were maintained in LD and then transferred to DD (days 0 to 44). At day 10, the recording was disrupted for about 45 hr. (**c**) Circadian periods of free-running activities in DD. The free-running period was estimated by χ2 periodogram from days 4–43 in DD. Bars indicate mean period ± s.e.m. (WT, n = 8; *Per2*E′$^{m/m}$, n = 10). ***P<0.0001, Student's t-test.

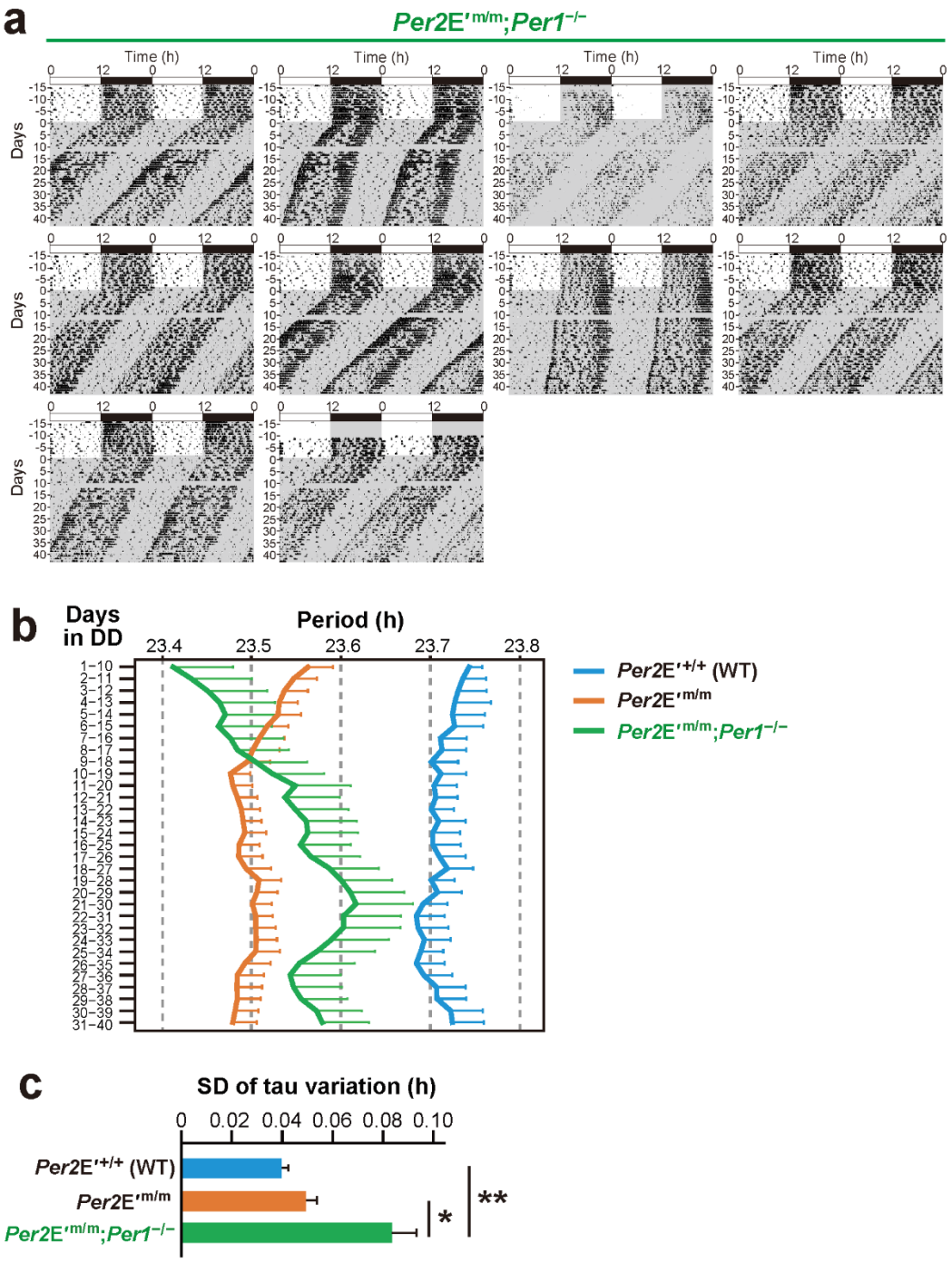

Supplementary Fig. 2 *Per2*E′$^{m/m}$;*Per1*$^{-/-}$ mice display an unstable free-running period of locomotor activity rhythms in DD. (**a**) Double-plotted actograms of *Per2*E′$^{m/m}$;*Per1*$^{-/-}$ mice. Animals were maintained in LD and then transferred to DD. At day 10, the recording was disrupted for about 45 hr. (**b**) Daily plots of tau at 10-day intervals in DD (mean ± s.e.m.) for Per2E′$^{+/+}$ (WT) (n = 8), Per2E′m/m (n = 10), and *Per2*E′$^{m/m}$;*Per1*$^{-/-}$ (n = 10). Tau was calculated with χ^2 periodogram. (**c**) Standard deviation (SD) of tau variations for 40 days in (**b**). Data indicate mean ± s.e.m. *P<0.05, **P<0.01, one-way ANOVA, Bonferroni *post hoc* test.

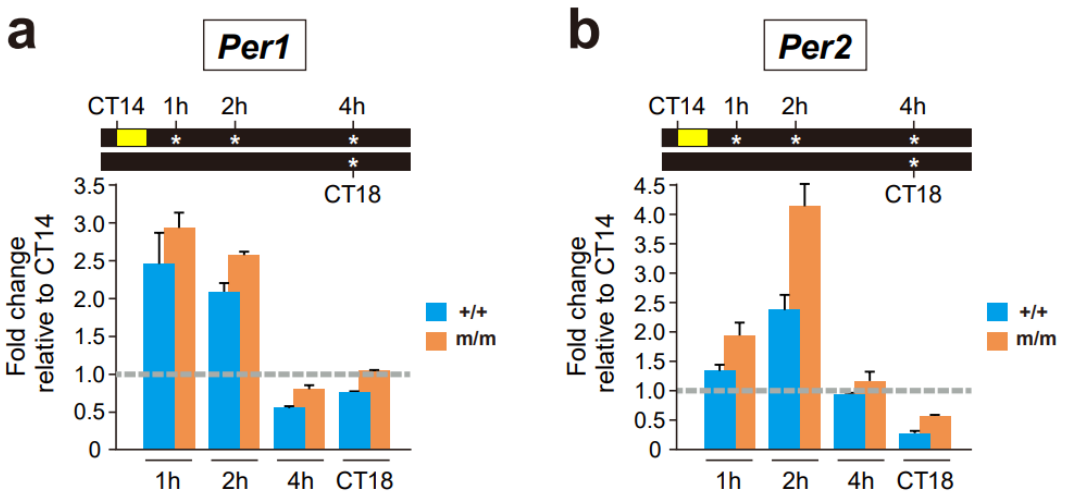

Supplementary Fig. 3 Expression profiles of *Per1* and *Per2* in the SCN of WT (+/+) and Per2E′$^{m/m}$ (m/m) mice after a 30-min light pulse exposure at CT14. Mice were sacrificed 1, 2, 4 h after the light onset. No-light-exposed animals at CT18 served as control groups. The SCN was dissected out by laser microdissection, and mRNA levels of *Per1* (**a**) and *Per2* (**b**) were determined by qRT-PCR and normalized to those of the ribosomal phosphoprotein P0 (Rplp0)-encoding gene. Data are plotted as means ± variation (n = 2 mice for each data point), relative to basal values at CT14. Note that the *Per2*E′$^{m/m}$ mutation augments light-induced expression of *Per2* but not *Per1*.

References

1. Kvon, EZ et al. Progressive loss of function in a limb enhancer during snake evolution. Cell 167, 633–642 e611 (2016).
2. Indjeian, VB et al. Evolving new skeletal traits by cis-regulatory changes in bone morphogenetic proteins. Cell 164, 45–56 (2016).
3. Whyte, WA et al. Master transcription factors and mediator establish superenhancers at key cell identity genes. Cell 153, 307–319 (2013).
4. Rosbash, M et al. Transcriptional feedback and definition of the circadian pacemaker in Drosophila and animals. Cold Spring Harb. Symp. Quant. Biol.72, 75–83 (2007).
5. Masri, S & Sassone-Corsi, P. The circadian clock: a framework linking metabolism, epigenetics and neuronal function. Nat. Rev. Neurosci. 14, 69–75 (2013).
6. Takahashi, JS. Transcriptional architecture of the mammalian circadian clock. Nat. Rev. Genet. 18, 164–179 (2017).
7. Hao, H, Allen, DL. & Hardin, PE. A circadian enhancer mediates PERdependent mRNA cycling in Drosophila melanogaster. Mol. Cell. Biol. 17, 3687–3693 (1997).
8. Gekakis, N. et al. Role of the CLOCK protein in the mammalian circadian mechanism. Science 280, 1564–1569 (1998).
9. Ueda, HR et al. System-level identification of transcriptional circuits underlying mammalian circadian clocks. Nat. Genet. 37, 187–192 (2005).

10. O’Neill, JS & Reddy, AB. Circadian clocks in human red blood cells. Nature 469, 498–503 (2011).
11. Edgar, RS et al. Peroxiredoxins are conserved markers of circadian rhythms. Nature 485, 459–464 (2012).
12. Yang, Z. & Sehgal, A. Role of molecular oscillations in generating behavioral rhythms in Drosophila. Neuron 29, 453–467 (2001).
13. Atobe Y. Mechanism of circadian oscillation of the mammalian core clock gene Per2. Doctoral dissertation. Kyoto Univ. (2015)
14. Zheng, B. et al. The mPer2 gene encodes a functional component of the mammalian circadian clock. Nature 400, 169–173 (1999).
15. Zheng, B. et al. Nonredundant roles of the mPer1 and mPer2 genes in the mammalian circadian clock. Cell 105, 683–694 (2001).
16. Bae, K. et al. Differential functions of mPer1, mPer2, and mPer3 in the SCN circadian clock. Neuron 30, 525–536 (2001).
17. Toh, KL. et al. An hPer2 phosphorylation site mutation in familial advanced sleep phase syndrome. Science 291, 1040–1043 (2001).
18. Yoo, SH. et al. A noncanonical E-box enhancer drives mouse Period2 circadian oscillations in vivo. Proc. Natl Acad. Sci. USA 102, 2608–2613 (2005).
19. Akashi, M., Ichise, T., Mamine, T. & Takumi, T. Molecular mechanism of cellautonomous circadian gene expression of Period2, a crucial regulator of the mammalian circadian clock. Mol. Biol. Cell 17, 555–565 (2006).

20. Koike, N. et al. Transcriptional architecture and chromatin landscape of the core circadian clock in mammals. Science 338, 349–354 (2012).
21. Noguchi, T., Ikeda, M., Ohmiya, Y. & Nakajima, Y. A dual-color luciferase assay system reveals circadian resetting of cultured fibroblasts by co-cultured adrenal glands. PLoS ONE 7, e37093 (2012).
22. Ono, D. et al. Dissociation of Per1 and Bmal1 circadian rhythms in the suprachiasmatic nucleus in parallel with behavioral outputs. Proc. Natl Acad. Sci. USA 114, E3699–E3708 (2017).
23. Myung, J. et al. GABA-mediated repulsive coupling between circadian clock neurons in the SCN encodes seasonal time. Proc. Natl Acad. Sci. USA 112, E3920–E3929 (2015).
24. Seluanov, A., Vaidya, A. & Gorbunova, V. Establishing primary adult fibroblast cultures from rodents. J. Vis. Exp. 44, e2033 (2010).
25. Tainaka, M., Doi, M., Inoue, Y., Murai, I. & Okamura, H. Circadian PER2 protein oscillations do not persist in cycloheximide-treated mouse embryonic fibroblasts in culture. Chronobiol. Int. 35, 132–136 (2018).
26. Fustin, JM. et al. RNA-methylation-dependent RNA processing controls the speed of the circadian clock. Cell 155, 793–806 (2013).
27. Yamazaki, S. & Takahashi, JS. Real-time luminescence reporting of circadian gene expression in mammals. Methods Enzymol. 393, 288–301 (2005).

28. Doi, M. et al. Gpr176 is a Gz-linked orphan G-protein-coupled receptor that sets the pace of circadian behaviour. Nat. Commun. 7, 10583 (2016).
29. Doi, M. et al. Circadian regulation of intracellular G-protein signaling mediates intercellular synchrony and rhythmicity in the suprachiasmatic nucleus. Nat. Commun. 2, 327 (2011).
30. Yamaguchi, Y. et al. Mice genetically deficient in vasopressin V1a and V1b receptors are resistant to jet lag. Science 342, 85–90 (2013).
31. Kiessling, S., Eichele, G. & Oster, H. Adrenal glucocorticoids have a key role in circadian resynchronization in a mouse model of jet lag. J. Clin. Invest. 120, 2600–2609 (2010).
32. Herzog, ED., Hermanstyne, T., Smyllie, NJ. & Hastings, MH. Regulating the Suprachiasmatic Nucleus (SCN) Circadian Clockwork: interplay between cell-autonomous and circuit-level mechanisms. Cold Spring Harb. Perspect. Biol. 9, a027706 (2017).
33. Okamura, H. Suprachiasmatic nucleus clock time in the mammalian circadian system. Cold Spring Harb. Symp. Quant. Biol. 72, 551–556 (2007).
34. Kadener, S., Menet, JS., Schoer, R. & Rosbash, M. Circadian transcription contributes to core period determination in Drosophila. PLoS Biol. 6, e119 (2008).

35. Liu, A. C. et al. Intercellular coupling confers robustness against mutations in the SCN circadian clock network. Cell 129, 605–616 (2007).
36. Pittendrigh, CS. & Daan, S. A functional analysis of circadian pacemakers in nocturnal rodents. III. Heavy water and constant light: homeostasis of frequency? J. Comp. Physiol. A 106, 267–290 (1976).
37. Ohta, H., Yamazaki, S. & McMahon, DG. Constant light desynchronizesmammalian clock neurons. Nat. Neurosci. 8, 267–269 (2005).
38. Winfree, AT. The Geometory of Biological Time, (Springer, New York, 2000).
39. Vitaterna, MH et al. The mouse Clock mutation reduces circadian pacemaker amplitude and enhances efficacy of resetting stimuli and phaseresponse curve amplitude. Proc. Natl Acad. Sci. USA 103, 9327–9332 (2006).
40. Liu, C., Weaver, DR., Strogatz, SH. & Reppert, SM. Cellular construction of a circadian clock: period determination in the suprachiasmatic nuclei. Cell 91, 855–860 (1997).
41. Herzog, ED., Takahashi, JS. & Block, GD. Clock controls circadian period in isolated suprachiasmatic nucleus neurons. Nat. Neurosci. 1, 708–713 (1998).

42. Nakamura, W., Honma, S., Shirakawa, T. & Honma, K. Clock mutation lengthens the circadian period without damping rhythms in individual SCN neurons. Nat. Neurosci. 5, 399–400 (2002).
43. Travnickova-Bendova, Z., Cermakian, N., Reppert, SM. & Sassone-Corsi, P. Bimodal regulation of mPeriod promoters by CREB-dependent signaling and CLOCK/BMAL1 activity. Proc. Natl Acad. Sci. USA 99, 7728–7733 (2002).
44. So, AY., Bernal, TU., Pillsbury, ML., Yamamoto, KR. & Feldman, BJ. Glucocorticoid regulation of the circadian clock modulates glucose homeostasis. Proc. Natl Acad. Sci. USA 106, 17582–17587 (2009).
45. Hastings, MH., Maywood, ES. & O'Neill, JS. Cellular circadian pacemaking and the role of cytosolic rhythms. Curr. Biol. 18, R805–R815 (2008).
46. Parsons, MJ. et al. The regulatory factor ZFHX3 Modifies Circadian function in SCN via an AT motif-driven axis. Cell 162, 607–621 (2015).
47. O'Neill, JS., Maywood, ES., Chesham, JE., Takahashi, JS. & Hastings, MH. cAMP-dependent signaling as a core component of the mammalian circadian pacemaker. Science 320, 949–953 (2008).
48. Lane, JM. et al. Genome-wide association analysis identifies novel loci for chronotype in 100,420 individuals from the UK Biobank. Nat. Commun. 7, 10889 (2016).

49. Hu, Y. et al. GWAS of 89,283 individuals identifies genetic variants associated with self-reporting of being a morning person. Nat. Commun. 7, 10448 (2016).
50. Jones, SE. et al. Genome-wide association analyses in 128,266 individuals identifies new morningness and sleep duration loci. PLoS Genet. 12, e1006125 (2016).

Chapter 2

Calcitonin receptor modulates body temperature rhythms in mammals

Introduction

The body temperature rhythm (BTR) is one of the most conspicuous outputs of the circadian clock[1-3] and is crucial for maintaining homeostasis in metabolism and sleep as well as entraining the peripheral clock in mammals[4-9]. In humans, body temperature increases during wakefulness and decreases during sleep[10]. As daily variations in BTR are robust and parallel fluctuations in locomotor activity rhythm (LAR), BTR is widely used to monitor circadian rhythms in mammals. The molecular mechanisms underlying the regulation of BTR remain largely uncharacterized, although a study in which subsets of neurons in the brains of rats were surgically ablated suggested that LAR and BTR are controlled by different output pathways that originate from the suprachiasmatic nucleus (SCN)[11]. In humans, body temperature fluctuates even when locomotor activity is restricted[12,13], and BTR and LAR can be experimentally dissociated, a phenomenon known as spontaneous internal desynchronization[14]. These accumulating data suggest that BTR is likely controlled separately from LAR. However, no molecular evidence supporting this possibility has been reported. Therefore, there is a critical need to identify genes that regulate BTR.

In the present study, I show that calcitonin receptor (*Calcr*) is expressed in the SCN and mediates BTR during the night (active phase for mice). Calcr is a member of the secretin family of GPCRs and is known to participate in calcium homeostasis in osteoclasts[15]. Since *Calcr* is not involved in LAR[16],

these findings provide the first molecular evidence that BTR is regulated separately from LAR.

Methods

Mouse strain

Mutant *Calcr* mice (*Calcr*^{tm1Dgen}) with a mixed genetic background involving 129P2/OlaHsd × C57BL/6J were obtained from the Mutant Mouse Regional Resource Center at the University of North Carolina (https://www.mmrrc.org) and backcrossed to C57BL/6J for 10 generations. The *Calcr*$^{+/-}$ mice were then intercrossed to produce homozygous null and wild-type progenies by in vitro fertilization. All of the animal experiments were performed according to protocols approved by the Animal Care and Experimentation Committee of Kyoto University.

Measurements of BTR and LAR

Single caged male littermate mice (aged 6 wk) were housed individually in light-tight ventilated closets in a temperature- and humidity-controlled facility. The animals were entrained on a LD cycle for at least 2 wk before the experiments. The core body temperatures of *Calcr*$^{+/+}$ and *Calcr*$^{-/-}$ mice (8 wk of age) were measured using a Thermochron iButton DS1921H (Maxim Integrated), which was inserted into the peritoneal cavity as described previously[17]. Following a week of convalescence, the mice were

maintained in either LD or DD. The body temperatures of the animals were measured every 20 min, and three measurements obtained in each nonoverlapping 60-min interval were then averaged to obtain a single value for each clock hour. To extract circadian trends, we averaged the data obtained at each time of day on three consecutive days and smoothed the data once using a three-point moving average. Locomotor activity was simultaneously detected with passive (pyroelectric) infrared sensors (Omron, FA-05 F5B), and the data were analyzed with ClockLab software (Actimetrics) developed on MatLab (Mathworks), as described elsewhere[17].

Mouse histology

In situ hybridization was performed with free-floating brain sections (30 mm thick) using either a [33P]-labeled or a digoxigenin labeled cRNA probe specific for mouse Calcr (nucleotides 670– 1168; NM_007588), as described previously[16]. Free-floating immunohistochemistry was also performed using 5 µg/mL anti-Calcr antibody (Abcam, ab11042), as described elsewhere[16], and immunoreactivity was visualized with a peroxidase-based Vectorstain Elite ABC kit (Vector Laboratories) with diaminobenzidine serving as the chromogen. For dual-label immunofluorescence, the free-floating sections were stained with 5 µg/mL anti-Calcr (rabbit polyclonal; Abcam, ab11042) along with either 4 µg/mL anti-Vipr2 (chicken polyclonal)[16], 1:1000 anti-VIP (guinea pig polyclonal; Abnova, PAB16648), or 0.2 µg/mL anti-AVP-associated neurophysin II (goat polyclonal; Santa Cruz Biotechnology, sc-

27093) antibodies. Immunoreactivity was visualized using Alexa 594-conjugated anti-rabbit IgG (1:1000; Life Technologies) and Alexa 488-conjugated anti-chicken, anti-guinea pig, or anti-goat IgG (1:1000; Life Technologies) antibodies. The nuclei were visualized by staining with 4,6-diamino-2-phenylindole (DAPI).

Results

Mouse Calcr is expressed in the SCN shell

Our laboratory and others reported previously that *Calcr* is highly expressed in the SCN in rats and mice. Importantly[16,18,19], this expression pattern is reproducibly observed in the Allen Brain Atlas[20]. I therefore further characterized Calcr expression in the SCN by in situ hybridization and immunohistochemistry (Fig. 1). I found that *Calcr* mRNA and Calcr protein were similarly distributed from the rostral to the caudal margins of the SCN (Fig. 1a-b). Topographically, the *Calcr* mRNA and protein signals in SCN were detected mainly in the dorsomedial area, a region corresponding to the SCN shell. To gain additional insight into the regional distribution of Calcr in the SCN shell, double immunostaining was performed with anti-Calcr and anti-arginine vasopressin (AVP) antibodies (Fig. 1d), the latter of which was used as a marker of the SCN shell[21]. I found that the distributions of AVP and Calcr partially overlapped in the SCN shell: Approximately 84% of the Calcr-positive cells expressed AVP, while ~65% of the AVP-positive cells

expressed Calcr (Fig. 1d). Double immunostaining was also performed using anti-Calcr and anti-VIP antibodies, the latter which delineates the SCN core. I found that VIP and Calcr did not colocalize (Fig. 1c), suggesting that Calcr is not expressed in the VIP-ergic SCN core[21]. Taken together, these findings show that Calcr expression is localized mainly to a part of the SCN shell that partially overlaps the AVP-expressing region of the SCN.

Mouse Calcr mediates body temperature fluctuations during the night

To determine whether Calcr is involved in mediating BTR, I used *Calcr* knockout mice that had been backcrossed to the C57BL/6J background for >10 generations. Using both in situ hybridization and anti-*Calcr* immunostaining, I confirmed that *Calcr* mRNA and protein were absent in the SCN of *Calcr* knockout mice (Fig. 2a). Importantly, *Calcr* knockout mice showed a normal free-running period of LAR as well as normal total locomotor activity. These observations are consistent with previously reported data[17] (Fig. 2b).

In LD conditions, the body temperature of wild-type mice fluctuates over each 24-h period[10]. During the daytime, when the mice were primarily resting, their body temperature gradually decreased during the early phase and increased during the later phase[22-24] (Fig. 2c). However, during the night, the animals' body temperature displayed bimodal peaks in the early night and at dawn, with a deep trough late in the night (i.e., midnight trough) (Fig. 2c). The midnight trough in body temperature has been reported

previously[24,25], and my data confirmed that the difference between the body temperatures at the early peak (22:00) and at the trough (4:00) was statistically significant (Fig. 2c, blue asterisk, [***] $P < 0.001$). Furthermore, the body temperature fluctuation patterns observed over the 24-h period, including the midnight trough, were very similar in LD and DD conditions, although the overall body temperatures were slightly lower in DD than in LD (Fig. 2d). These data indicate that the patterns of temporal fluctuations in body temperature are controlled by the endogenous clock.

Although I found that the body temperatures of both wild-type and *Calcr* knockout mice fluctuated over a 24-h period, they were significantly different at midnight (Fig. 2c-d, black asterisks, [*] $P < 0.05$). Specifically, the body temperatures of wild-type mice showed a deep trough at midnight (Fig. 2c-d, blue asterisk, [***] $P < 0.001$), whereas the body temperatures of *Calcr* knockout mice lost the characteristic trough and remained relatively unchanged during the night in both LD (Fig. 2c) and DD (Fig. 2d) conditions (Fig. 2c-d, orange asterisk, [*] $P < 0.05$ for LD and *n.s.* for DD). These data indicate that the lack of Calcr expression causes a shallow midnight trough in body temperature, suggesting that Calcr is required for body temperature fluctuations, particularly during the night (the active phase of mice).

Because body temperature may be increased by locomotor activity, I speculated that higher levels of locomotor activity result in the higher body temperatures observed in *Calcr* knockout mice. To examine this possibility, I compared fluctuations in locomotor activity between wild-type and *Calcr*

knockout mice in both LD (Fig. 2e) and DD (Fig. 2f) conditions; however, there was no significant difference in locomotor activity between the two groups. Therefore, we concluded that Calcr specifically mediates body temperature fluctuations during the night but does not affect locomotor activity rhythms.

Discussion

Calcitonin receptors mediate daily BTR

Daily BTR is essential for homeostatic functions, such as metabolism and sleep[4]. Several lines of evidence suggest that BTR is controlled separately from locomotor activity rhythms[11-14]; however, no molecular evidence supporting this model has been reported to date. Given that several mouse mutants that have defects in BTR also have defects in locomotor activity rhythms[22-24], it is crucial to find genes that specifically regulate daily BTR.

Here, I provide the first evidence that *Calcr* plays a role in mediating BTR during the active phase in mice. First, I found that Calcr is expressed in the brain's central clock neurons (Fig. 1). Second, although *Calcr* mutants showed almost no fluctuations in body temperature during the active phase (Figs. 2), they showed normal LAR (Fig. 2b,e,f). These observations thus revealed that Calcr plays an important role in daily BTR during the active phase but not in LAR. This molecular evidence therefore substantiates the premise that the daily profiles of body temperature and locomotor activity

are controlled separately.

A possible contribution of nonclock cells to BTR

I found that Calcr is present not only in the SCN but also in regions outside the SCN, such as the subparaventricular zone (SPZ), the medial preoptic area (MPO), and the arcuate nucleus (ARC) (data not shown). These findings are consistent with those of previous studies[18,19]. The MPO is involved in thermoregulation[26], and ablation of the dorsal SPZ causes abnormal BTR but not abnormal locomotor rhythm in rats[11]. Therefore, Calcr function may not be limited to clock cells, and it is possible that Calcr neurons at extra-SCN sites may contribute to mediating BTR.

The role of body temperature fluctuations during the night

The mouse BTR includes two peaks, one in the early night and one at dawn, with a trough at midnight. As BTR is highly influenced by animal rest–activity states, BTR patterns temporally correlate with those of LAR. Therefore, it is reasonable to speculate that the trough in the middle of the dark phase seen in wild-type mice could be due simply to the animals' resting and may perhaps be a passive consequence of the activity burst that occurs during the early part of the night. However, given that *Calcr* deletion resulted in a flat body temperature throughout the night without affecting locomotor activity (Fig. 2c–f), these results strongly suggest that the midnight body temperature trough is genetically and endogenously programmed and not

merely a consequence of decreased locomotor activity. Interestingly, mice deficient in the nuclear receptor Rev-erbα also show a reduced body temperature fluctuation amplitude as well as a reduced midnight trough[24]. Notably, it appears likely that human body temperature also drops during the active phase (at approximately 3:00 pm)[39]. Thus, my data raise the possibility that the midnight trough in body temperature may play a proactive role in homeostatic regulation, much like physiology and metabolism regulation; this would be an interesting subject for a future study.

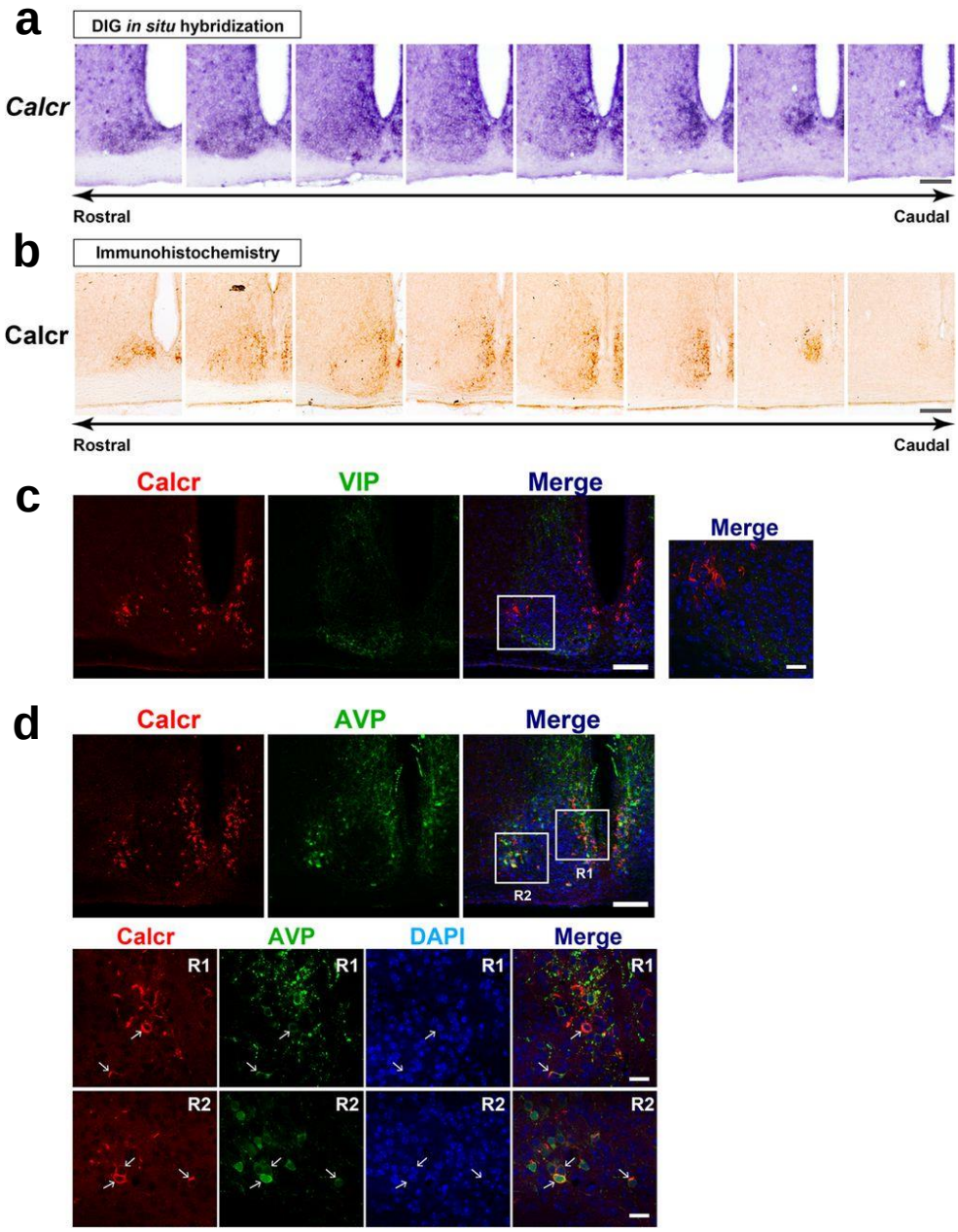

Fig. 1 The mouse Calcr is expressed in the SCN shell. (**a**,**b**) Topographical distribution of *Calcr* mRNA (**a**) and Calcr protein (**b**) in serial coronal brain sections covering the entire mouse SCN in the rostral–caudal direction. Bar, 100 µm. (**c**) Double-label confocal immunofluorescence of Calcr and VIP in the mouse SCN. The merged image shows combined images of Calcr-based (red), VIP-based (green), and 4,6-diamino-2-phenylindole (DAPI)-based nuclear staining (blue). The boxed area is enlarged in the *right* panel. Bars: *left*, 100 µm; *right*, 20 µm. (**d**) Double-label confocal immunofluorescence of Calcr and arginine vasopressin (AVP). The boxes indicate the regions enlarged in the *bottom* panels. The arrows indicate cells double-immunolabeled for Calcr and AVP. Bars: *top*, 100 µm; *bottom*, 20 µm.

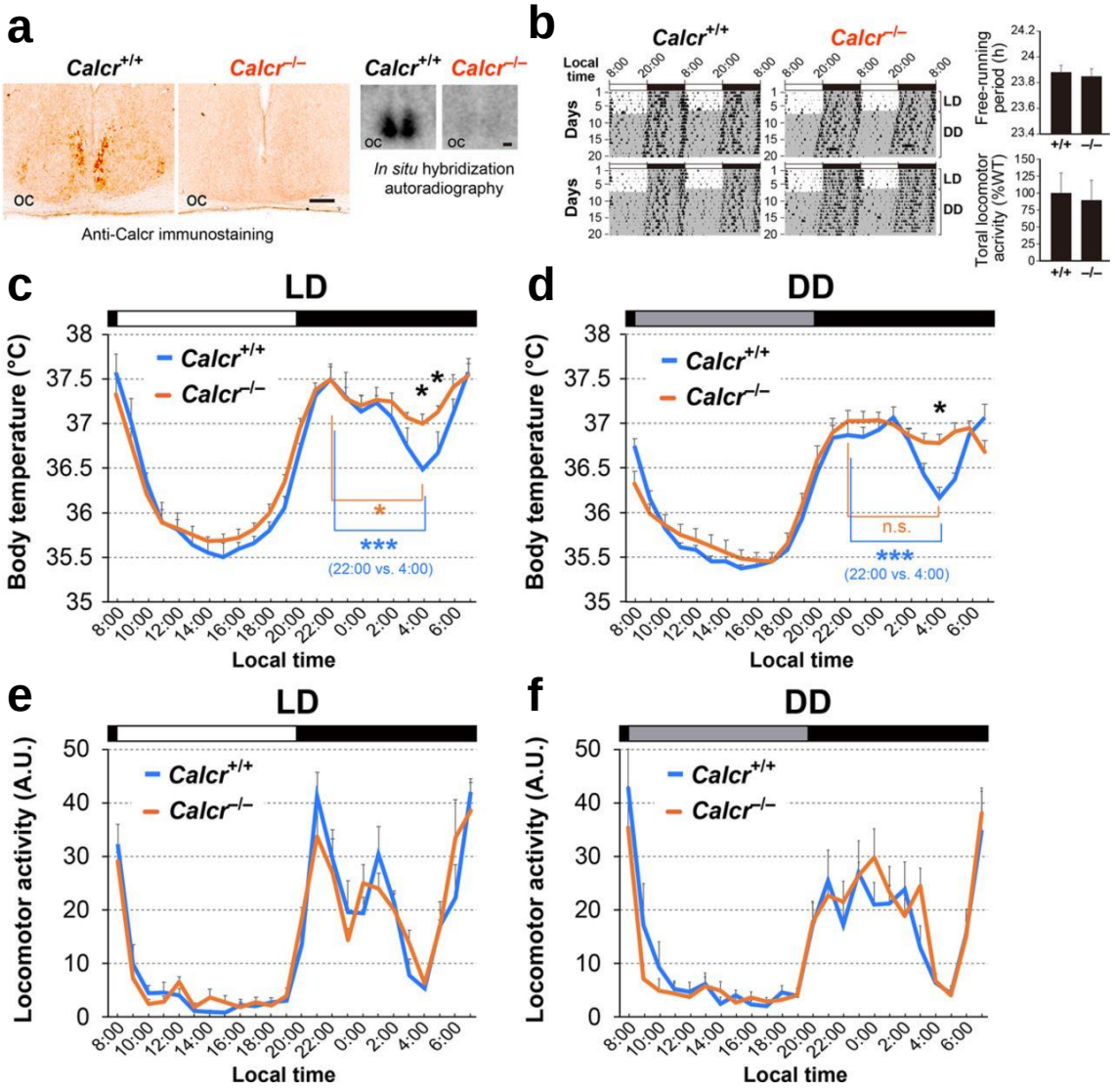
a
Calcr+/+
Calcr−/−
OC
Anti-Calcr immunostaining
In situ hybridization autoradiography
b
Local time
Days
LD
DD
Free-running period (h)
Toral locomotor acrivity (%WT)
+/+
−/−
c
LD
Body temperature (°C)
Local time
(22:00 vs. 4:00)
d
DD
n.s.
e
LD
Locomotor activity (A.U.)
f
DD

Fig. 2 *Calcr* knockout mice exhibit an abnormal body temperature during the active phase. (**a**) Immunohistochemistry (*left*) and radioisotopic in situ hybridization (*right*) confirm the deficiency of Calcr protein and transcript levels in $Calcr^{-/-}$ mice in the SCN. Bar, 100 µm. (oc) Optic chiasm. (**b**) Double-plotted actograms of C57BL/6J-backcrossed $Calcr^{+/+}$ and $Calcr^{-/-}$ mice over 7 d in LD and 13 d in DD. The periods of darkness are indicated by gray backgrounds. The bar graphs indicate the mean ± SEM of the free-running periods of $Calcr^{+/+}$ and $Calcr^{-/-}$ mice and their relative total locomotor activity per day. The values were determined based on a 10-d interval taken after 3 d in DD. $n = 6$ (both genotypes). $P = 0.521$ for period; $P = 0.806$ for activity, unpaired *t*-test. (*C*,*D*) Body temperatures of $Calcr^{+/+}$ and $Calcr^{-/-}$ mice in LD (**c**) and DD (**d**), as measured by intra-abdominally implanted thermometers. The body temperatures at each time of day for three consecutive days in LD (**c**) or DD (**d**) were averaged and smoothed once with a three-point moving average. The values shown are the mean ± SEM. $n = 5$ mice for each data point. (Black asterisk) $P < 0.05$, $Calcr^{+/+}$ versus $Calcr^{-/-}$ (two-way ANOVA with Bonferroni *post hoc* test); (blue asterisks) $P < 0.001$, 22:00 versus 4:00 in $Calcr^{+/+}$ mice; (orange asterisk) $P < 0.05$, 22:00 versus 4:00 in $Calcr^{-/-}$ mice; (n.s.) not significant (one-way ANOVA with Bonferroni post hoc test). (**e**, **f**) The temporal profiles of $Calcr^{+/+}$ and $Calcr^{-/-}$ locomotor activity in LD (**e**) and DD (**f**). The locomotor activities of $Calcr^{+/+}$ and $Calcr^{-/-}$ mice at each time of day on three consecutive days were averaged and plotted as the mean ± SEM. $n = 5$ mice per genotype.

References

1. Aschoff J. Circadian control of body temperature. J. Therm. Biol. 8, 143–147 (1983).
2. Krauchi K. How is the circadian rhythm of core body temperature regulated? Clin. Auton. Res. 12, 147–149 (2002).
3. Weinert D. Circadian temperature variation and ageing Ageing. Res. Rev. 9, 51–60 (2010).
4. Refinetti R, & Menaker M. The circadian rhythm of body temperature. Physiol Behav 51, 613–637 (1992).
5. Gilbert SS, et al. Thermoregulation as a sleep signalling system. Sleep Med. Rev. 8, 81–93 (2004).
6. Krauchi K. The human sleep-wake cycle reconsidered from a thermoregulatory point of view. Physiol. Behav. 90, 236–245 (2007).
7. Krauchi K. The thermophysiological cascade leading to sleep initiation in relation to phase of entrainment. Sleep Med. Rev. 11, 439–451 (2007).
8. Buhr ED, Yoo SH, & Takahashi JS. Temperature as a universal resetting cue for mammalian circadian oscillators. Science 330, 379–385 (2010).
9. Morf J, & Schibler U. Body temperature cycles: gatekeepers of circadian clocks. Cell Cycle 12, 539–540 (2013).

10. Duffy JF et al. Later endogenous circadian temperature nadir relative to an earlier wake time in older people. Am. J. Physiol. 275, R1478–R1487 (1998).
11. Saper CB, Lu J, Chou TC, & Gooley J. The hypothalamic integrator for circadian rhythms. Trends. Neurosci. 28, 152–157 (2005).
12. Smith RE. Circadian variations in human thermoregulatory responses. J. Appl. Physiol. 26, 554–560 (1969).
13. Gander PH, Connell LJ, & Graeber RC. Masking of the circadian rhythms of heart rate and core temperature by the rest-activity cycle in man. J. Biol. Rhythms 1, 119–135 (1986).
14. Lavie P. Sleep-wake as a biological rhythm. Annu. Rev. Psychol. 52, 277–303 (2001).
15. Masi L, Brandi ML. Calcitonin and calcitonin receptors. Clin Cases Miner Bone Metab. 4, 117–122 (2007).
16. Doi M et al. Gpr176 is a Gz-linked orphan G-protein-coupled receptor that sets the pace of circadian behaviour. Nat. Commun. 7, 10583 (2016).
17. Yamaguchi Y et al. Mice genetically deficient in vasopressin V1a and V1b receptors are resistant to jet lag. Science 342, 85–90 (2013).
18. Nakamoto H et al. Localization of calcitonin receptor mRNA in the mouse brain: coexistence with serotonin transporter mRNA. Brain Res Mol. Brain. Res. 76, 93–102 (2000).

19. Becskei C et al. Immunohistochemical mapping of calcitonin receptors in the adult rat brain. Brain Res. 1030, 221–233 (2004).
20. Lein ES et al. Genome-wide atlas of gene expression in the adult mouse brain. Nature 445, 168–176 (2007).
21. Abrahamson EE, & Moore RY. Suprachiasmatic nucleus in the mouse: retinal innervation, intrinsic organization and efferent projections. Brain Res. 916, 172–191 (2001).
22. Shiromani PJ et al. Sleep rhythmicity and homeostasis in mice with targeted disruption of mPeriod genes. Am. J. Physiol. Regul. Integr. Comp. Physiol. 287, R47–R57 (2004).
23. Nagashima K et al. The involvement of Cry1 and Cry2 genes in the regulation of the circadian body temperature rhythm in mice. Am. J. Physiol. Regul. Integr. Comp. Physiol. 288, R329–R335 (2005).
24. Gerhart-Hines Z et al. The nuclear receptor Rev-erbα controls circadian thermogenic plasticity. Nature 503, 410–413 (2013).
25. Wolff G, Duncan MJ, & Esser KA. Chronic phase advance alters circadian physiological rhythms and peripheral molecular clocks. J. Appl. Physiol. 115, 373–382 (2013).
26. Morrison SF, & Nakamura K. Central neural pathways for thermoregulation. Front. Biosci. 16, 74–104 (2011).
27. Patke A, et al. Mutation of the human circadian clock gene CRY1 in familial delayed sleep phase disorder. Cell 169, 203–215.e13 (2017).

Chapter 3

Temporal relationships between body temperature and behaviour revealed by thermographic imaging

Introduction

LAR and BTR have been used to detect circadian rhythms in living animals because they are both robust and easy to be measured. However, there are still unfilled opportunities for close analysis of LAR and BTR. For the purpose of detecting circadian locomotor activity, LAR is usually detected by either infrared sensor or running wheel[1-3]. Yet, these methods cannot detect non-locomotor movements (i.e., activities which do not involve moving from place to place), including feeding, drinking, grooming, and postural adjustments. As for the time-series quantification of body temperature, measurements are usually performed by implanting a thermal sensor into abdominal cavity of animals[1,4,5]. These measures, however, require surgery. Moreover, a sensor device is often large for small laboratory animals such as mice, making these experiments highly invasive. In addition, long-term measurement of BTR with high time-resolution over several days has been difficult due to limited data storage performance of thermal sensor devices. These limitations have hampered elucidation of how LAR and BTR are temporally correlated to each other.

To solve these technical problems, I developed a new method able to trace simultaneously body surface temperature (BST) and body movements (BM). I took thermographic video images of mice using an infrared camera and calculated BST. First, I verified that mice show a clear circadian rhythm of BST. Then, to allow comparisons between BST and BM, I calculated BM from the same video images. These simultaneous measurements of BST and

BM, notably, led to the identification of increased BST prior to the onset of locomotor activity. Intriguingly, in this pre-locomotion period, mice exhibit non-locomotor movements, suggesting that non-locomotor movements are required for mice to warm up before initiation of locomotor activity. In addition to these findings, in this study, I developed a machine learning-based approach to detect drinking and feeding behaviours from video images. These data demonstrate that the potential utility of real-time video imaging-based analysis of animal behaviours.

Methods

Animals

All animal studies were performed with protocols approved by the animal experimentation committee of Kyoto University. I used male C57BL/6J mice. Before experiments, all animals were acclimated for at least 2 weeks in a 12-h light-dark cycle.

Infrared imaging

For thermographic analysis, mice were housed individually in experimental cages and monitored using a thermal imaging camera (Tau 2, FLIR Systems). A Camera Link frame grabber (ThermalCapture Grabber USB, TEAX Technology) was installed on the camera to extract digital images. To clearly detect body surface temperature of mice, back hair was removed with razors.

Thermal video images of the entire cage were recorded at a resolution of 640 × 512. The area of mouse is roughly 4000 pixels. Thermal images were collected at 30 Hz. To reduce computation time, video recordings were down-sampled to 2 frames per second for all analyses.

Calculating BST from thermal images

I defined BST as the 200th highest value of each frame. To correct for internal measurement error, I used room temperature (median value of each frame) as the reference point. For each frame, the magnitude of the internal error was calculated as the difference between raw and 600-sec (1200-point) moving average value of room temperature. BST was then corrected by subtracting the internal error calculated. Since BST can fluctuate greatly depending on postures of mice, BST data were smoothed once with a 120-point moving average.

Calculating BM from thermal images

To automatically find positions of mice from thermal images, I first binarized thermal images using 4000th highest values of frames as thresholds. Then, I clustered pixels of binary image using DBSCAN (RAPIDS cuML library, eps=2.24, min_samples=18), and the largest cluster was defined as the area of mouse. The centroid of the area of mouse was used as the reference point. Body movement (BM) was defined as the distance of reference points between frames. Then, I used 60-sec (120-point) moving median of BM

(mBM) for the classification of behaviour into three different categories, locomotor movement (mBM > 10), non-locomotor movement (0.8 < mBM ≤ 10), and resting (mBM ≤ 0.8). Transitions from resting to movement were extracted from data by selecting the events in which the animal's behaviours change from resting (defined 80% or more resting for 500 sec) to movement (defined continuous locomotor or non-locomotor movement for 300 sec). Extracted events were hierarchically clustered by Ward's method (scikit-learn library) using Euclidean distances among transition events data. For this cluster analysis, resting is set to 0, non-locomotor movement is set to 1, and locomotor movement is set to 2.

Detecting feeding and drinking behaviour from thermal images

Automated detection of feeding and drinking was performed using DeepLabCut, an efficient method for pose estimation with deep neural networks[6]. I created and trained a DeepLabCut model for each animal using 150 video frames with manual labelling (nose, ears, neck, and back). The nose position of mouse was then estimated for all images. If the estimated nose position was within the range of the food position for 2.5 sec (i.e. five consecutive frames), I judged it as feeding, and if the estimated nose position was within the range of the water bottle tip position for 1.5 sec, I judged it as drinking.

Results

BST measures using thermal video imaging

To measure BST in a non-invasive way at high time-resolution, I employed infrared camera-based thermal video imaging of living animals (Fig. 1a). In previous reports, the highest body temperature of mouse was defined as BST[7,8]. However, I noticed that the highest values tend to be various depending on postures of animal. Thus, in this study, I defined BST as the 200th highest value (Fig. 1a). Raw BST values were smoothed once with a 120-point (60-sec) moving average after internal measurement errors were corrected (see Methods). BST of C57BL/6J mice displayed a clear circadian rhythm of bimodal peaks, one in the early night and at dawn, with a deep trough at midnight (Fig. 1b-c), which is in parallel with temperature at abdominal cavity of mice (Chapter 2 Fig. 2c-d)[1,4].

Identification of BST elevation with non-locomotor movements before initiation of locomotor activity

I next devised a method for quantifying body movement (BM) from thermal images. As shown in Fig 2a, thermal images exhibit relatively high temperatures not only in the location of mouse but also in the areas where the mouse was previously located (Fig 2a, white arrow). Therefore, binarization by thresholding was insufficient to calculate the location of mouse accurately. To solve this problem, in addition to binarization, a clustering method called DBSCAN[9] was used to distinguish the location of

mouse from regions of non-interest (Fig. 2a). The centroid of the area of mouse was used as the reference point. BM was defined as the distance of reference points between frames. BM also displayed a clear circadian rhythm of bimodal peaks, one in the early night and at dawn, with a deep trough at midnight, similar to locomotor activity measurements with a non-video-based recording system (Fig. 2b-c, Chapter 2 Fig. 2 e-f). As expected, a strong positive correlation was observed between BST and BM ($R = 0.819 \pm 0.128$) (Fig. 2d), which is consistent with previous reports[10,11]. However, besides this gross correlation, I noticed that BST was not constantly low, rather variable, when BM values were low (Fig. 2d). Thus, I next more closely analyzed the temporal relationship between BST and BM when mean BM value was lower than 2 pixels per sec. Interestingly, as shown in Fig 2e, this analysis led to the identification of increased BST prior to the onset of locomotor activity. In this pre-locomotion period, BST was gradually increased without apparent locomotor activity (Fig. 2e, middle), but appreciable BM values of about 1-10 pixels per sec were captured within this period (Fig. 2e, bottom), suggesting that BST elevation occurs in association with "non-locomotor" movement. To test this association in depth, I classified behaviours of mice into three distinct states according to BM using 120-point (60-sec) moving median of BM (mBM) value; resting ($mBM \leq 0.8$), non-locomotor movement ($0.8 < mBM \leq 10$), and locomotor movement ($mBM > 10$). Real-time video imaging confirmed that mice do not move at all during resting (see #1 in Fig 2e), do move their bodies or groom

themselves at the same location during non-locomotor movement (see #2 in Fig 2e), and move around the cage during locomotor movement (see #3 in Fig 2e). Then, to analyze relationship between BST and BM, I extracted all transition events from resting to movement from all video data (n = 124 events from 4 mice, Fig. 2f). Overall, BST started to increase at the transitions of resting to movement (Fig. 2f). To perform systematic analysis, I conducted unsupervised hierarchical clustering analysis of BM states around the transitions (from −500 sec to +700 sec) and found that the patterns of emergent order of BM states can be separated into three distinct clusters: cluster I (resting → non-locomotor movement → locomotor movement), cluster II (resting → non-locomotor movement), and cluster III (resting → non-locomotor movement → resting). Noticeably, there is no events showing an immediate direct transition from resting to locomotor movement, indicating that non-locomotor movements always precede locomotor movements. Nevertheless, non-locomotor movements are not always accompanied by locomotor movements. These patterns of behaviour are consistent with a previous report[12]. As expected, BST was decreased after transition from non-locomotor movement to resting (Fig. 2g, cluster III). Interestingly, elevated BST values in clusters I and II were almost comparable to each other, while total BM activity after the transition of cluster I is significantly higher than that of cluster II (Fig. 2h). These results suggest that non-locomotor movement is an independent mechanism of thermogenesis, comparable to active movement.

Detection of feeding and drinking behaviour from video imaging

In addition to LAR and BTR, various other physiological phenomena are controlled by an internal circadian clock[13,14]. Thus, I developed a system to detect drinking and feeding behaviour from video imaging. To do so, I determined the nose position of animal by using DeepLabCut algorithm, which allows efficient and accurate pose estimation[6]. First, I randomly extracted frames and labeled them by body parts (nose, neck, ears, and back) as shown in Fig. 3a. Next, I trained DeepLabCut models and estimated positions of the body parts for all images. Feeding and drinking were judged by whether the estimated nose position overlapped with the area of food source and of a tip of the water bottle, respectively (Fig. 3a). The frequency of feeding and drinking displayed clear circadian rhythms of bimodal peaks, one in the early night and at dawn, with a deep trough at midnight (Fig. 3b-d), which is consistent with previous reports[14,15].

Discussion

By measuring BM and BST with an infrared camera, I visualized previously unknown BST elevation in mice that occurs in close association with non-locomotor activity. Crucially, active locomotor movements were always preceded by non-locomotor activity-associated BST elevation, suggesting that non-locomotor activity is required for mice to warm up before initiation of locomotor activity. Interestingly, non-locomotor movements were not

always accompanied by locomotor activity, suggesting that non-locomotor activity-associated BST elevation may have a role independent from locomotion. Because non-locomotor movements that were not followed by active locomotor movements were mainly observed during the light phase, in which mice are primarily resting (Supplementary Fig. 1), it is tempting to speculate that non-locomotor movement may have a role in thermogenesis during rest to keep homeostasis of body temperature.

Although non-locomotor movements, such as grooming and postural adjustments, appear to be important for body temperature regulation, I should mention that non-locomotor movements cannot explain all BST variations observed during light/resting phase. Indeed, small but non-negligible BST variations were displayed by mice at rest without appreciable non-locomotor movements, suggesting the presence of BM-independent body temperature regulation. One possible BM-independent mechanism may involve brown adipose tissue (BAT). BAT produces heat in response to sympathetic activation without physical activity[16]. Another possible mechanism is skeletal muscle-mediated thermogenesis[17,18]. BM-independent BST fluctuation may be caused by skeletal muscle activity that cannot be captured by the video-based method. In addition, skeletal muscle has recently been shown to have a heat-producing mechanism that does not involve muscle contraction[17], which may also contribute to BM-independent BST elevation.

Previous human studies report that not only high-intensity exercise,

such as sports and fitness-related activities, but also activities of daily living, such as sitting, standing, walking, and fidgeting, increase energy expenditure and mediate resistance to weight gain with overfeeding[19,20]. Interestingly, energy expenditure increases by ~50% with only fidgeting-like activities while seated[20]. In this study, I showed that non-locomotor movements of mice increase body temperature to the levels almost comparable to or slightly less than those observed during locomotor movement. Therefore, studying the role of non-locomotor movement-associated thermogenesis in mice may help to understand the impact of non-exercise activities on daily regulation of energy homeostasis.

Circadian clocks orchestrate multiple different physiological rhythms in a well-synchronized manner[13,21], but little is known about how these separate rhythms are regulated coordinately. Interestingly, previous studies in mice and humans support the notion that BTR and LAR are regulated separately[22-25]. In line with this, in the Chapter 2, I revealed that Calcr is involved in LAR-independent BTR control. In addition, it was recently revealed that SCN neurons that directly project to thirst neurons in the OVLT (organum vasculosum lamina terminalis) control water intake just before resting period[14], suggesting that LAR and drinking rhythm are coordinately regulated. These recent findings all highlight the increasing importance of simultaneous measurement of multiple physiological activity rhythms to elucidate coordinated circadian outputs. In this study, I showed that BST, BM, feeding, and drinking can be simultaneously measured by thermal video

imaging and automated behavioural analyses. Thus, this method may be instrumental to understand inter-relationship between these independent circadian behaviours of mice. In this study, I roughly classified BM into three states: resting, non-locomotor movement, and locomotor movement. However, behaviours of mice are more complex than classified, as mice exhibit other behaviours, such as grooming, nest-building, defecation, and urination. Development of a system to detect these behaviours automatically and elucidation of temporal relationships between these behaviours are the subject of further study.

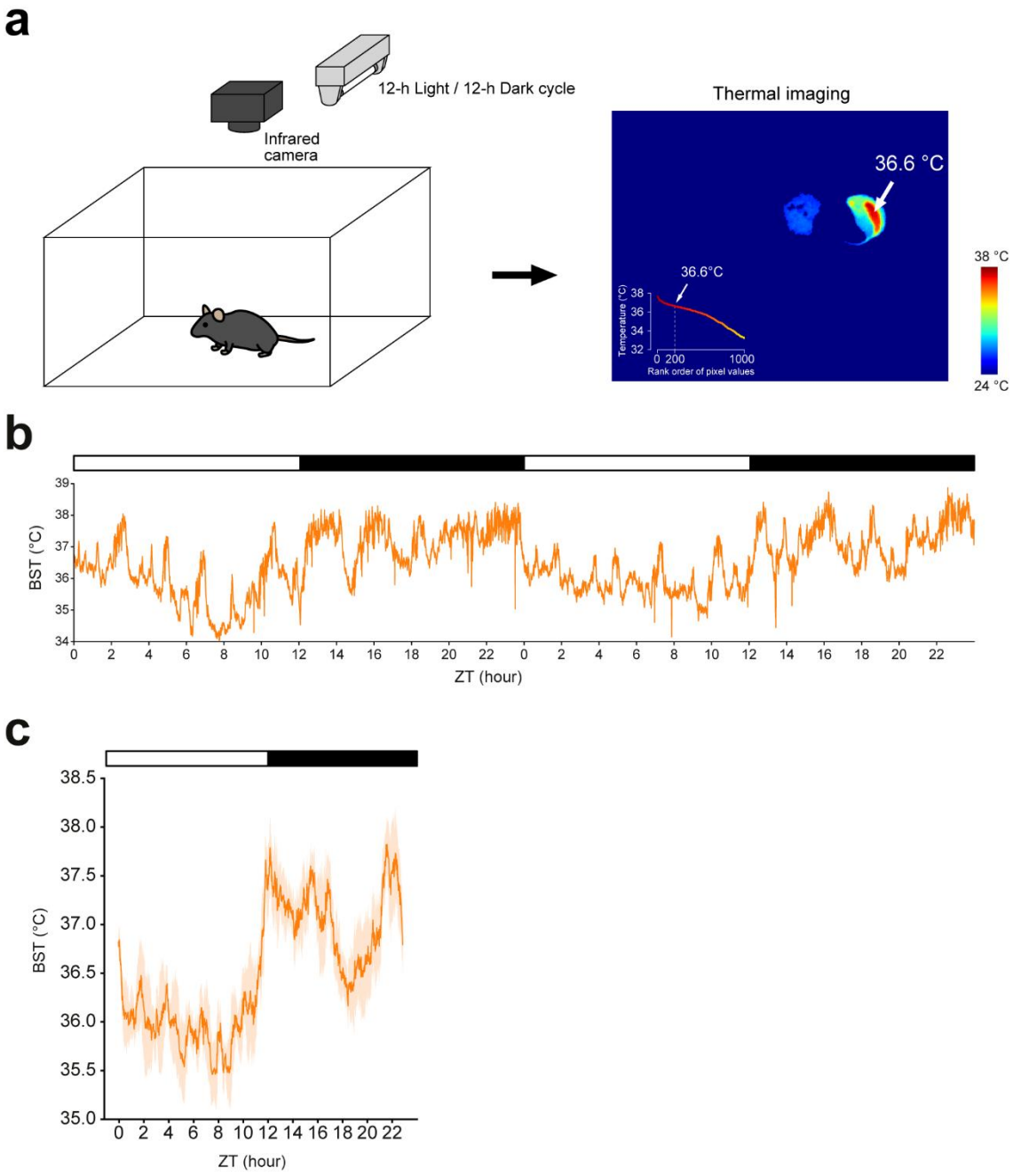

Fig. 1 Infrared video camera-based monitoring of circadian body surface temperature (BST). (**a**) Schematic representation of video imaging and representative thermography. The inset indicates temperatures of top 1000 pixels on mouse. Arrows indicate the 200th highest temperature. (**b**) Representative BST records of C57BL/6J mice under light/dark (LD) cycle for 2 days. BST was calculated for every 0.5 second. BST data were smoothed once with a 120-point moving average. (**c**) Averages of 3 days recording of BST. Data are presented as mean ± SEM. n = 4 mice.

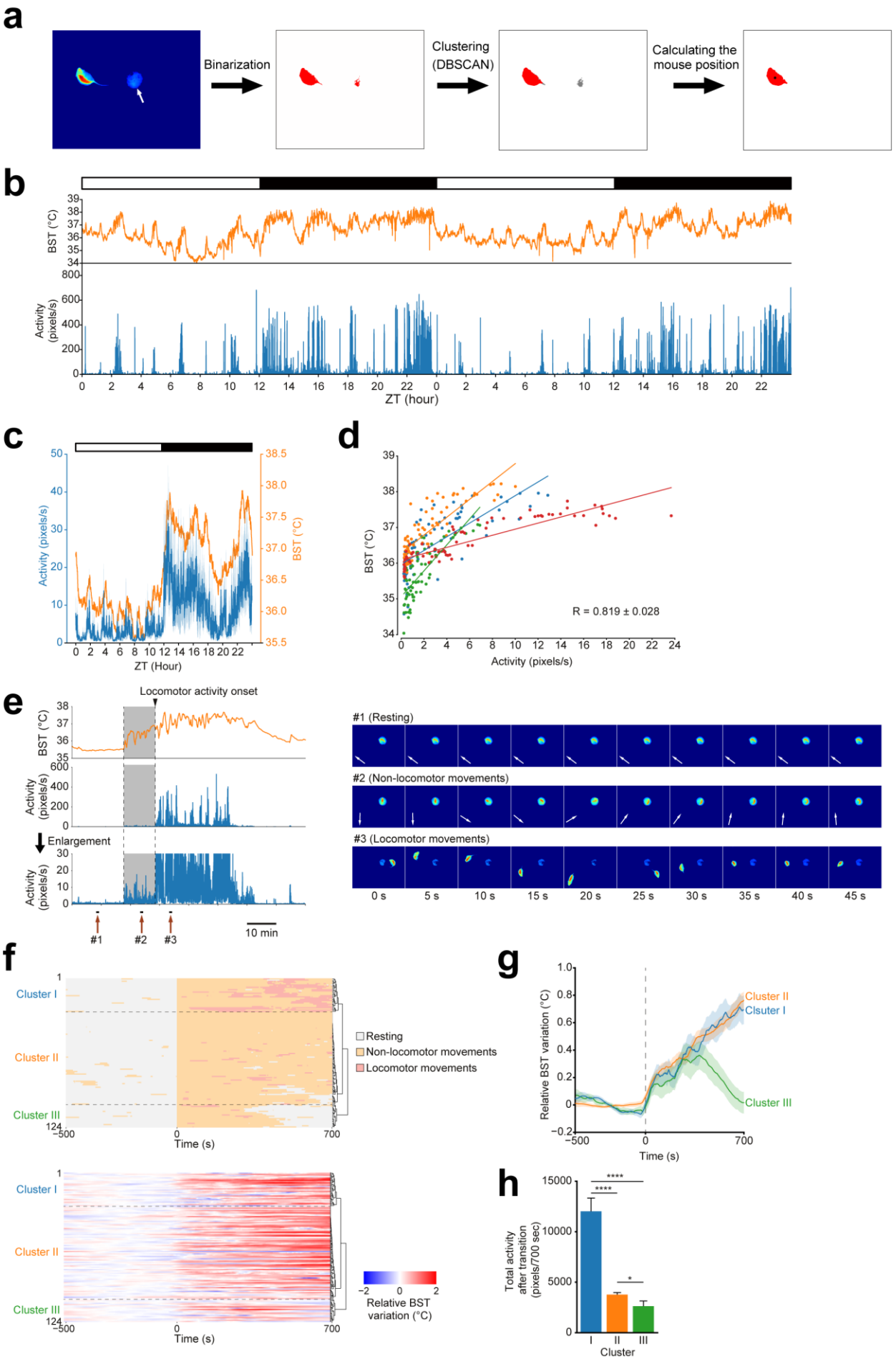
a
Binarization
Clustering
(DBSCAN)
Calculating the
mouse position
b
BST (°C)
Activity
(pixels/s)
ZT (hour)
c
Activity (pixels/s)
BST (°C)
ZT (Hour)
d
BST (°C)
R = 0.819 ± 0.028
Activity (pixels/s)
e
Locomotor activity onset
BST (°C)
Activity
(pixels/s)
Enlargement
#1
#2
#3
10 min
#1 (Resting)
#2 (Non-locomotor movements)
#3 (Locomotor movements)
38 °C
24 °C
0 s
5 s
10 s
15 s
20 s
25 s
30 s
35 s
40 s
45 s
f
Cluster I
Cluster II
Cluster III
Resting
Non-locomotor movements
Locomotor movements
Time (s)
Relative BST
variation (°C)
g
Relative BST variation (°C)
Cluster II
Clsuter I
Cluster III
Time (s)
h
Total activity
after transition
(pixels/700 sec)
Cluster

Fig. 2 Infrared video camera-based monitoring of circadian body movement (BM). (**a**) Representative imaging analysis for the determination of mouse position. The process involves binarization, clustering (DBSCAN), and calculating mouse position. A black dot on the red segments indicates the centroid of the area of mouse. A white arrow indicates the areas open but previously warmed by mouse. (**b**) Representative BST and BM records of C57BL/6J mice under LD cycle for 2 days. (**c**) Averages of 3 days recording of BM and BST. Data are presented as mean ± SEM. $n = 4$ mice. (**d**) Scatter plots showing the relationship between BST and BM. Each data point represents averages of BST (y-axis) and BM (x-axis) for every 1 hour. Each color represents an individual mouse ($n = 4$). Diagonal lines represent linear fitting of the data of each animal. (**e**) Representative BST and BM profiles under different BM states. A period of increase in BST prior to the onset of locomotor activity is highlighted by yellow background. Image data on the right show representative mouse positions under resting (#1), non-locomotor movements (#2), and locomotor movements (#3). White arrows indicate the nose-tail directions of the mouse. (**f**) Alignments of all resting to movement transition events ($n = 124$ events for 4 mice). The upper and lower graphs indicate BM and BST data, respectively. All the events were clustered into 3 groups. Time 0, time of transition. For BST, average of 500 seconds before transition was set to 0. (**g**) Time course of average BST increase from resting-to-movement transitions in each cluster. (**h**) Total BM activity after the transition. $*P < 0.05$, $****P < 0.0001$, Welch ANOVA and post-hoc Games-Howell test.

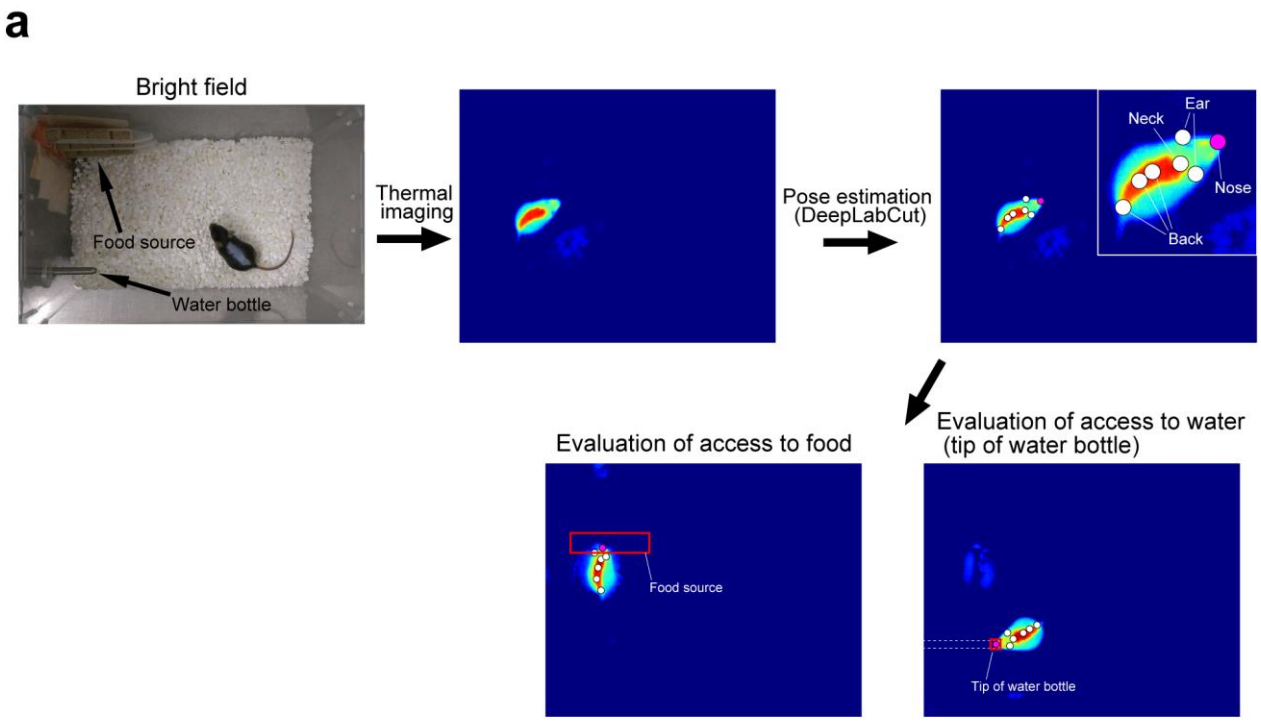
a
Bright field
Food source
Water bottle
Thermal imaging
Pose estimation (DeepLabCut)
Ear
Neck
Nose
Back
Evaluation of access to food
Food source
Evaluation of access to water (tip of water bottle)
Tip of water bottle

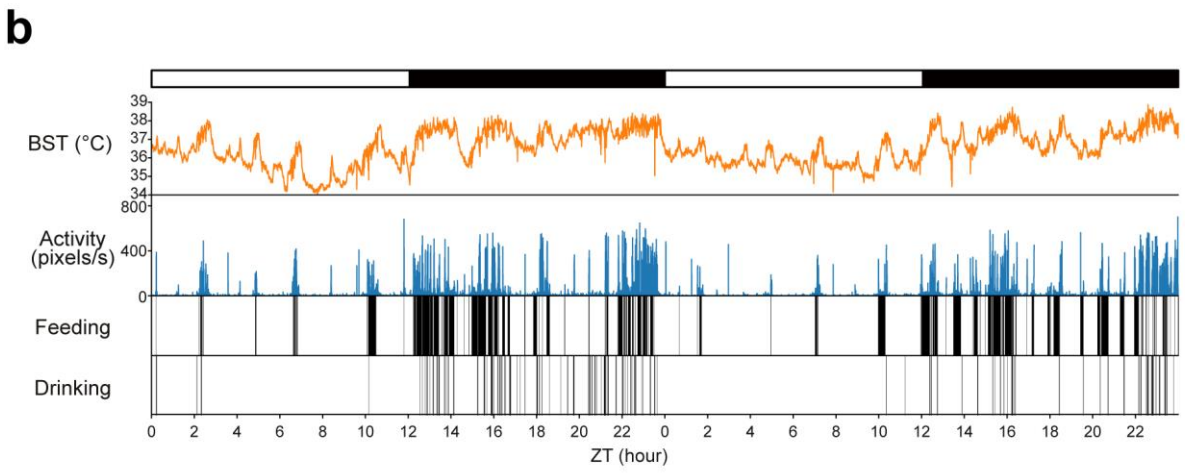
b
BST (°C)
Activity (pixels/s)
Feeding
Drinking
ZT (hour)

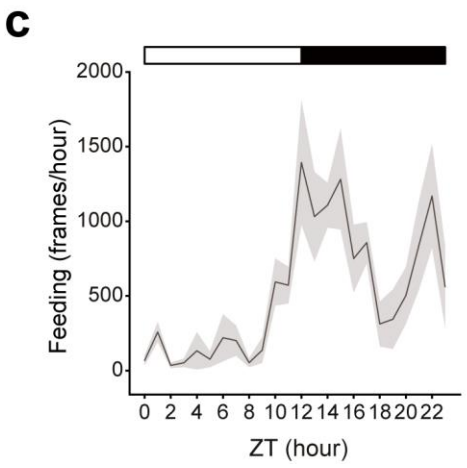
c
Feeding (frames/hour)
ZT (hour)

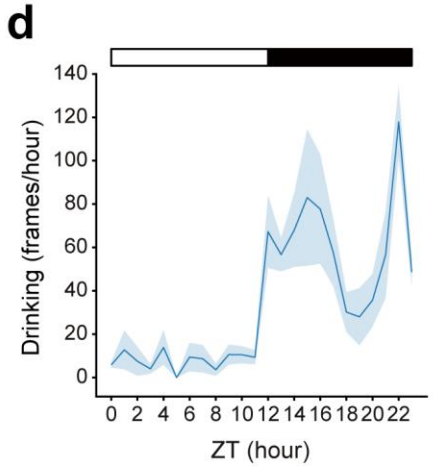
d
Drinking (frames/hour)
ZT (hour)

Fig. 3 Infrared video camera-based monitoring of circadian feeding and drinking behaviour. (**a**) Representative imaging analysis for the determination of feeding and drinking behaviour. The process involves thermal imaging, pose estimation (DeepLabCut), and evaluation of access to food or water (tip of water bottle). (**b**) Representative BST, BM, feeding, and drinking records of C57BL/6J mice under LD cycle for 2 days. (**c**, **d**) Averages of 3 days recording of feeding (**c**) and drinking (**d**). Data are presented as mean ± SEM. *n* = 4 mice.

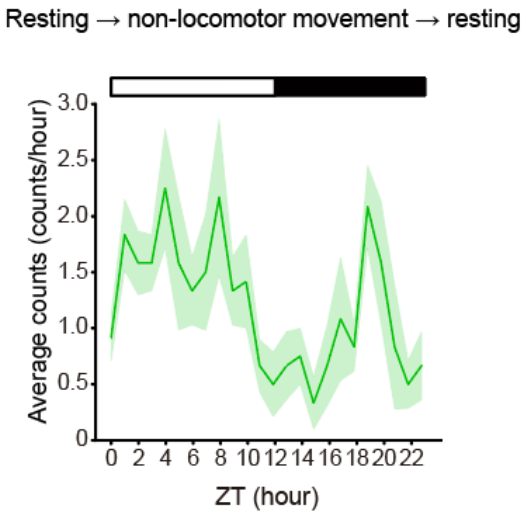

Supplementary Fig. 1 Averages of 3 days recording of non-locomotor movements which were not accompanied by locomotor movements. Data are presented as mean ± SEM. n = 4 mice. Transitions from resting to non-locomotor movement were extracted from data by selecting the events in which the animal's behaviours change from resting to continuous non-locomotor movement for more than 60 sec.

References

1. Yamaguchi, Y. et al. Mice genetically deficient in vasopressin V1a and V1b receptors are resistant to jet lag. Science 342, 85–90 (2013).
2. D'Alessandro, M et al. A tunable artificial circadian clock in clock-defective mice. Nat. Commun. 6, 8587 (2015).
3. Collins, B. et al. Circadian VIPergic neurons of the suprachiasmatic nuclei sculpt the sleep-wake cycle. Neuron 108, 486-499 (2020)
4. Gerhart-Hines Z, et al. The nuclear receptor Rev-erbα controls circadian thermogenic plasticity. Nature 503, 410–413 (2013).
5. Conti B. et al. Transgenic mice with a reduced core body temperature have an increased life span. Science 314, 825-828 (2006)
6. Mathis A. et al. DeepLabCut: markerless pose estimation of user-defined body parts with deep learning. Nat. Neurosci. 21, 1281–1289 (2018).
7. Takahashi TM. et al. A discrete neuronal circuit induces a hibernation-like state in rodents. Nature 583, 109-114
8. van der Vinne V. et al. Continuous and non-invasive thermography of mouse skin accurately describes core body temperature patterns, but not absolute core temperature. Sci. Rep. 6, 28788 (2020).
9. Ester M. et al. A density-based algorithm for discovering clusters in large spatial databases with noise. AAAI press. 226-231 (1996).

10. Refinetti R. Relationship between the daily rhythms of locomotor activity and body temperature in eight mammalian species. Am. J. Physiol. 277, 1493-1500 (1999).
11. Weinert D. & Waterhouse J. Diurnally changing effects of locomotor activity on body temperature in laboratory mice. Physiol. Behav. 63, 837-843 (1998).
12. Liu D. et al. A common hub for sleep and motor control in the substantia nigra. Science 367, 440-445 (2020).
13. Patke A. et al. Molecular mechanisms and physiological importance of circadian rhythms. Nat. Rev. Mol. Cell Biol. 21, 67-84 (2020).
14. Gizowski C. et al. Clock-driven vasopressin neurotransmission mediates anticipatory thirst prior to sleep. Nature 537, 685-688 (2016).
15. Yasumoto Y et al. Free access to a running-wheel advances the phase of behavioral and physiological circadian rhythms and peripheral molecular clocks in mice. PLOS ONE 10, e0116476 (2015).
16. Cannon, B. & Nedergaard, J. Brown adipose tissue: function and physiological significance. Physiol. Rev. 84, 277–359 (2004)
17. Bal NC et al. Sarcolipin is a newly identified regulator of muscle-based thermogenesis in mammals. Nat. Med. 18, 1575-1579 (2012)
18. Periasamy M et al. Skeletal muscle thermogenesis and its role in whole body energy metabolism. Diabetes Metab. 41, 327-336 (2017)

19. Levine JA, Eberhardt NL, Jensen MD. Role of nonexercise activity thermogenesis in resistance to fat gain in humans. Science 283:212–214 (1999).
20. Levine JA, Schleusner SJ, Jensen MD. Energy expenditure of nonexercise activity. Am. J. Clin. Nutr. 72, 1451-1454 (2000).
21. Hastings M, O'Neill JS & Maywood ES. Circadian clocks: regulators of endocrine and metabolic rhythms. J. Endocrinol. 195, 187-198 (2007).
22. Saper CB, Lu J, & Chou TC, Gooley J. The hypothalamic integrator for circadian rhythms. Trends Neurosci. 28, 152–157 (2005).
23. Smith RE. Circadian variations in human thermoregulatory responses. J Appl. Physiol. 26, 554–560 (1969).
24. Gander PH, Connell LJ, & Graeber RC. Masking of the circadian rhythms of heart rate and core temperature by the rest-activity cycle in man. J. Biol. Rhythms 1, 119–135 (1986).
25. Lavie P. Sleep-wake as a biological rhythm. Annu. Rev. Psychol. 52, 277–303 (2001).

Acknowledgements

First of all, I wish to express sincere thanks to Prof. Masao Doi and Prof. Hitoshi Okamura, for their direction and kind encouragement throughout my graduated study.

I am grateful to all the member of Doi's lab for their advice and help. In particular, I appreciate the technical assistance and contributions of Dr. Iori Murai, Dr. Yuta Atobe, and Mr. Hida Hayashi.

I thank my parents for their support and encouragement. Without their support I would not have accomplished this thesis.